Polymer Chemistry

REVIEW

View Article Online
View Journal | View Issue

Cite this: *Polym. Chem.*, 2016, **7**, 3783

Theoretical simulations of nanostructures self-assembled from copolymer systems

Zhanwen Xu, Jiaping Lin,* Qian Zhang, Liquan Wang and Xiaohui Tian

Copolymer systems can self-assemble into diverse nanostructures, which have gained significant attention because of their diverse and expanding range of practical applications, such as in microelectronic materials, optics and optoelectronics. Theoretical simulations offer a useful approach for the investigation of the evolution and formation of nanostructures and for determining their structure–property relationships. In this article, we highlight notable recent advances in simulation investigations of the nanostructures formed by the self-assembly of linear and nonlinear copolymers. We then focus on the theoretical simulations of the structure–property relationships of copolymer systems. The relationship between the nanostructures and their functional properties, including photovoltaic, optical and mechanical properties, is emphasized. Finally, we suggest directions for the further development of nanostructures formed by copolymer systems, especially regarding theoretical simulations of these systems. In addition, taking full advantage of the nanostructural feature, promising applications are suggested.

Received 26th March 2016,
Accepted 4th May 2016

DOI: 10.1039/c6py00535g

www.rsc.org/polymers

1. Introduction

Copolymers consist of two or more chemically distinct polymers covalently bonded together. The constituent blocks that are chemically incompatible tend to segregate into different phases. However, the covalent linkage between blocks restricts this phase separation to the length of the polymer molecules (typically tens of nanometres). Consequently, copolymers self-assemble into a diverse range of fascinating nanoscale structures.[1] The nanostructures self-assembled from copolymers present tremendous potential for technological applications, because they allow for the preparation of materials with photovoltaic, electrical, optical and mechanical properties tailored

Shanghai Key Laboratory of Advanced Polymeric Materials, State Key Laboratory of Bioreactor Engineering, Key Laboratory for Ultrafine Materials of Ministry of Education, School of Materials Science and Engineering, East China University of Science and Technology, Shanghai 200237, China. E-mail: jlin@ecust.edu.cn

Zhanwen Xu

Zhanwen Xu was born in Fujian Province, China, in 1989. He received his Bachelor's Degree in Materials Physics from East China University of Science and Technology (ECUST) in 2012. He is currently a doctoral candidate in Materials Science and Engineering at ECUST under the supervision of Professor Jiaping Lin, undertaking the theoretical simulations of copolymer systems.

Jiaping Lin

Jiaping Lin received his bachelor's and master's degrees from Shanghai Jiao Tong University, and Ph.D. from East China University of Science and Technology (ECUST, 1993). Then, he got a postdoctoral fellowship from the Japan Society for the Promotion of Science (JSPS), the Lise-Meitner fellowship of Fonds zur Förderung der wissenschaftlichen Forschung (FWF), and worked as a postdoctoral researcher at the Tokyo Institute of Technology and the University of Linz in Austria, respectively. Returning home from abroad in 1997, he has been at ECUST ever since then. He became a full professor in 1999. His current research interests include macromolecular self-assembly, biomaterials and liquid crystalline polymers.

in a "bottom up" manner.[2–6] Appropriate control of these structures can significantly improve the functional properties of these copolymer systems. Ultimately, numerous opportunities exist for designing new nanostructured materials with enhanced functional properties.

Nanostructures self-assembled from copolymer systems, have been the subject of intensive studies. Over the past few decades, substantial progress has been achieved in this field.[7,8] Due to the increased number of controlled parameters, nanostructures and their phase behaviours have become richer and more complex for copolymer self-assembly. However, understanding the copolymer self-assembly process is not sufficient to prepare advanced materials for applications using the "bottom up" approach. Characterizing these structures and gaining insight into the underlying mechanism governing the self-assembly remain challenging.[9,10] Therefore, the design of self-assembled structures of copolymers is largely empirical work. Thus, theoretical simulations have emerged as an important tool for understanding the self-assembly behaviours.

Over the last decade, increasing attention has been focused on theoretical simulations that can reproduce and predict the nanostructures self-assembled from copolymer systems. Theoretical simulations enable researchers to gain detailed thermodynamic and dynamic information on self-assembled nanostructures, which is difficult to deduce from experimental measurements. Furthermore, the structure–property relationship of a copolymer self-assembly can also be successfully predicted by theoretical simulations.

To date, many studies report experimental observations of nanostructures, whereas studies using theoretical simulations are relatively limited. Therefore, a systematic summary of the simulation studies regarding polymeric nanostructures is of significance. This type of review may provide guidance for further experimental investigations and deepen our understanding of the nature of the self-assembly process. On the other hand, there are few reports on the functional properties of these nanostructures, such as their photovoltaic properties. From these perspectives, we provide an overview of the theoretical simulations of nanostructures self-assembled from copolymer systems, as well as the functional properties of these nanostructures.

The review is organized as follows. In section 2, we briefly introduce the simulation methods used for investigating a copolymer self-assembly, including particle-based methods and field-based methods. In this section, we do not aim to provide detailed descriptions of each method; instead, the basic principles, advantages, and disadvantages of the methods are presented. For more detailed information, readers are referred to relevant articles and books. In sections 3, 4 and 5, we review nanostructures formed by linear and non-linear copolymers, respectively, studied using these simulation methods. In section 6, simulation investigations of the structure–property relationship of copolymer self-assemblies are reviewed. In each section, most of the simulation results are compared with experimental observations to highlight the validity of the simulation method and to facilitate an understanding of the simulation results. In section 7, a concluding remark is presented. We discuss the current challenges and the future directions of the developments in theoretical simulations of copolymer self-assemblies.

2. Modelling and simulation techniques

The length-scales of the copolymer self-assemblies are too large to be handled by any all-atomistic simulation technique. In fact, for nanostructures self-assembled from copolymers, it is not necessary to consider all chemical details. Therefore, it is better to resort to applying mesoscale approaches. Generally, mesoscale approaches can be grouped into particle-based methods and field-based methods.[11,12]

2.1 Particle-based methods

In particle-based mesoscale approaches, a group of monomers is replaced by one interaction centre based on the coarse-grained model. In a simulation box, this group of monomers is represented by a particle or bead. With bonding interactions

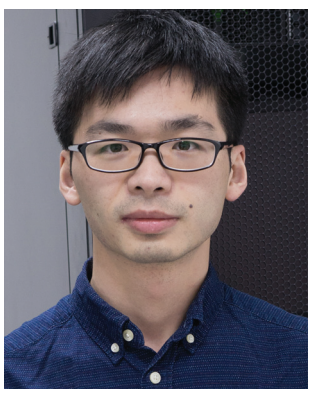

Qian Zhang

Qian Zhang was born in Jiangxi Province, China, in 1989. He received his Bachelor's Degree in Polymer Materials and Engineering from East China University of Science and Technology (ECUST) in 2010. He is currently a doctoral candidate in Materials Science and Engineering at ECUST under the supervision of Professor Jiaping Lin, undertaking the theoretical simulations of self-assembly in polymeric systems.

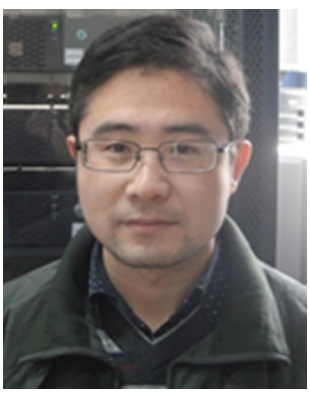

Liquan Wang

Liquan Wang was born in Zhejiang, China, in 1982. He received his Ph.D. degree under the supervision of Professor Jiaping Lin in Materials Science and Engineering from ECUST in 2011. Now he is working as an associate professor at the School of Materials Science and Technology of ECUST. His research interest is focused on the theoretical simulations of complex polymer systems.

and non-bonding interactions between different beads, the coarse-grained copolymer systems evolve into equilibrium states. There are four classical particle-based mesoscopic methods that can simulate the equilibrium states: coarse-grained molecular dynamics (CGMD), Brownian dynamics (BD), dissipative particle dynamics (DPD) and Monte Carlo simulations (MC).

In particle based methods of CGMD, BD and DPD, the evolution of particles is described by Newton's equations of motion:

$$m_i \frac{\mathrm{d}^2 \vec{r}_i(t)}{\mathrm{d}t^2} = \vec{F}_i(t) \quad (1)$$

where m_i, $\vec{r}_i$ and $\vec{F}_i$ represent the mass, the position of the ith particle, and the acting force on it, respectively. In CGMD, the interaction force $\vec{F}$ between different beads can simply be described by the non-bonded LJ potential and the bonded FENE potential.[13–16] These simple models are suitable for studying the self-assembly of general copolymers without any atomic detail. In another more accurate approach, the interaction parameters can be derived from an all-atom simulation with the following static methods: Boltzmann inversion, iterative Boltzmann inversion or inverse Monte Carlo.[17] With the coarse-graining potential, the time step used in CGMD can be tens of femtoseconds, which is much longer than that used in all-atom molecular dynamics. BD is a modification of molecular dynamics that is coupled to a Langevin thermostat.[18] In BD, a friction force $(-\gamma \vec{p}_i)$ and a random force $\left(\sigma \vec{\zeta}_i\right)$ are added into the non-bonded interaction force

$$\vec{F}_i(t) = \sum_{j \neq i} \vec{F}_{ij}^{\mathrm{C}}(t) - m_i \gamma \frac{\mathrm{d}\vec{r}_i(t)}{\mathrm{d}t} + \sigma \vec{\zeta}_i(t) \quad (2)$$

where γ denotes the friction constant, σ is the constant that can be obtained from γ with the Einstein relationship, and $\vec{\zeta}_i(t)$ is a Gaussian random noise term. Because of the additional friction force and random force in BD, the solvent molecules can be removed in the simulation of copolymer solutions. This approximation guarantees a high-efficiency simulation. However, the energy and momentum are no longer conserved, which implies that there are no hydrodynamic effects in BD simulation systems. DPD, introduced by Hoogerbrugge and Koelman, is a simulation technique based on soft particles. The soft particle is not regarded as an atom or molecule but a cluster of molecules.[19–21] DPD is similar to BD in which the standard canonical MD is augmented by dissipative and random forces between particles, representing the integrated effects of a coarse-grained fluid medium. However, in contrast to the BD method, both the additional dissipative and random forces in DPD are pairwise:

$$\vec{F}_i = \sum_{j \neq i} (\vec{F}_{ij}^{\mathrm{C}} + \vec{F}_{ij}^{\mathrm{D}} + \vec{F}_{ij}^{\mathrm{R}}) \quad (3)$$

where $\vec{F}_{ij}^{\mathrm{C}}$, $\vec{F}_{ij}^{\mathrm{D}}$ and $\vec{F}_{ij}^{\mathrm{R}}$ represent the conservative force, dissipative force and random force between the ith and jth particles, respectively. The additional forces are pairwise, which guarantees the conservation of momentum. Therefore, the macroscopic behaviour of a DPD system is hydrodynamic.[22] In contrast to the particle-based techniques discussed above that allow the prediction of the time evolution of a system of interacting particles, a Monte Carlo simulation generates a series of configurations according to their probability in a chosen ensemble using a Markov chain.[23,24] MC can be performed with a lattice model or an off-lattice model. MC simulations within a lattice model are faster than off-lattice simulations. Most MC simulations of copolymers, either in bulk or under confinement, are performed within a lattice model.[25]

2.2 Field-based methods

In field-based approaches, the polymer is represented by a statistical density field. The Hamiltonian or energy of the system is then expressed as a function of density fields rather than as a function of particle coordinates. Several mesoscale field-based approaches have been developed based on this idea. The frequently used methods, including the time-dependent Ginzburg–Landau (TDGL) method, dynamic density functional theory (DDFT) and self-consistent field theory (SCFT), are introduced here.

TDGL is a method at the simplest mesoscopic level, modelling polymer systems using a phenomenological expression for the free energy.[26] In this method, the dynamics of microphase separation for copolymer systems can be described by the following equation for a conserved order parameter:

$$\frac{\partial \phi}{\partial t} = M \nabla^2 \frac{\partial F[\phi]}{\partial \phi} + \eta(r,t) \quad (4)$$

where the order parameter ϕ is chosen as the local composition difference between different components, M is a phenomenological mobility coefficient, $F[\phi]$ is the free energy functional and $\eta(r,t)$ is a random noise term. With the calculation of the time-dependent local concentration, the structural evolution of the copolymer self-assembly can be obtained. To simplify TDGL, the cell dynamic method (CDM) was derived from the discretized TDGL equation. This model reproduces the growth kinetics of the TDGL model. Combining

Xiaohui Tian

Xiaohui Tian received his bachelor's and master's degrees from Nanjing University in 1985 and 1988 and has been a faculty member since then. He received his Ph.D. degree from the Mendeleev University of Chemical Technology, Russia, in 1995. He has been at ECUST since 1999, and has been a full professor since 2006. His research interests are metal coordination polymers and optical properties of organic molecules.

Gaussian mean-field statistics with a TDGL model, the DDFT method also models the behaviour of polymer fluids with the time evolution of conserved order parameters.[27–29] However, in contrast to TDGL, the free energy is not truncated; instead, it retains the full polymer path integral numerically. Therefore, it allows obtaining detailed information about a specific polymer system beyond simply the Flory–Huggins parameter and the mobilities. In contrast to the phenomenological methods, SCFT reformulates the partition function Z of the particle-based model in terms of a field-theoretical Hamiltonian $H[\phi,\omega]$:[30,31]

$$Z = \int D[\phi] \int D[\omega] \exp(-H[\phi,\omega]) \quad (5)$$

where ϕ is the density field and ω is the conjugate field. In principle, this general procedure is an exact reformulation of equilibrium properties, which can be estimated without invoking further approximations. SCFT has found widespread applications for the prediction of the equilibrium structures of copolymer systems both in bulk and under confinement. The main advantage of this popular technique over phenomenological, free-energy functional-based approaches is its ability to predict structures as well as the free energy and conformational entropy. Therefore, it can be used to map out the phase diagrams of copolymers with a complex architecture.

Investigations of copolymer self-assemblies involve a wide range of time and length scales, leading to an expensive computational cost. Furthermore, the ordered nanostructures are developed from an equilibrium state to an out of equilibrium state. Multiscale modelling methods, including multiscale molecular simulations and hybrid particle-continuum approaches, have been proposed to solve this problem. Multiscale molecular simulations are the methods using which the parameters used in the particle-based mesoscale approaches are calculated according to lower scale (atomistic) simulations.[17,32] Another strategy is the hybrid simulation method that combines particle-based methods with field methods. Recently, Kawakatsu *et al.* developed a hybrid particle-field simulation technique combining molecular dynamics and SCFT.[33,34] Using the hybrid method, they performed a series of simulations on a homogeneous homopolymer melt and a lamellar phase of a diblock copolymer melt. The results calculated by the hybrid method were consistent with the results calculated from classical MD simulations. However, when combining simulation methods at different length scales, many technical problems must be solved, for example, how to satisfy the mass, momentum, and energy conservation in the coupling of various methods.

3. Self-assembly of linear block copolymers

Linear block copolymers in which each molecule consists of two or more blocks joined in linear arrangements have been widely investigated due to their applications. The self-assembly behaviours of linear block copolymers are strongly affected by the number of blocks, the block type and the block sequence. In this section, the existing simulation studies of linear block copolymers, including AB diblock copolymers, ABA triblock copolymers and ABC triblock copolymers, are presented. The self-assembled nanostructures in bulk and confined systems and the corresponding ordering kinetics of linear block copolymers are discussed. By comparing the self-assembly behaviours of different linear block copolymers, we demonstrate the influence of molecular architecture on the self-assembled structures.

3.1 AB diblock copolymers

Diblock copolymers, as the simplest block copolymers composed of two chemically different blocks linked at their ends, have been extensively studied. A variety of nanostructures such as lamellae (L), gyroids (G), cylinders (C) and spheres (S) have been observed in diblock copolymer melts, as shown in Fig. 1(a).[35,36] These structures can be controlled by varying the chemical composition of the block copolymers or the segregation between blocks (*via* the molecular weight or the Flory–Huggins interaction parameter). While the composition of the AB diblock copolymer is symmetric, the melts segregate into a lamellar phase with flat interfaces. As the volume fractions of the diblock become asymmetric, nanostructures with curved interfaces are formed, causing the nanostructure to vary from gyroids to cylinders, then to spheres. In addition, there is a small window for the *Fddd* phase (denoting orthorhombic, space group 70, or O^{70}) in the region of the gyroid phase. The *Fddd* phase was predicted as an equilibrium structure in the phase diagram of diblock copolymers by Tyler *et al.* using SCFT.[37] Because the location of the *Fddd* phase in the weak segregation limit region is near the order–disorder transition

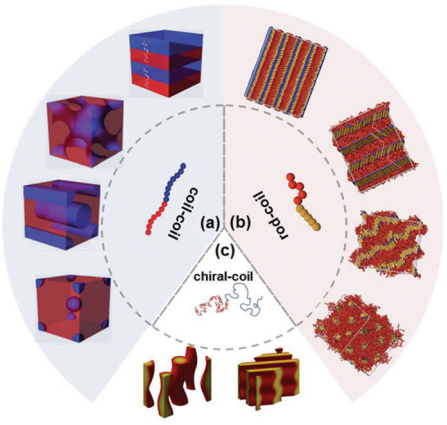

Fig. 1 (a) Schematic illustration of nanostructures of a coil–coil diblock copolymer. Reproduced with permission from ref. 35. Copyright 2014, The Royal Society of Chemistry. (b) Nanostructures of rod–coil diblock copolymers. Reproduced with permission from ref. 55. Copyright 2010, The Royal Society of Chemistry. (c) Two new chiral morphologies self-assembled from a diblock copolymer with a single chiral block. Reproduced with permission from ref. 69. Copyright 2013, American Physical Society.

(ODT), it was not observed experimentally in copolymer systems until the theoretical prediction. Following the prediction of the theoretical simulation, Takenaka *et al.* provided experimental evidence for the existence of the *Fddd* microdomain structure, which was discovered in a PS-*b*-PI diblock copolymer melt.[38,39]

Most theoretical simulations of diblock copolymers have focused on the ideal monodisperse AB diblock copolymer system. However, the polydispersity of the block length of block copolymers, parameterized as the polydispersity index (PDI), is well-known to influence nanostructures and macroscopic properties of copolymers. Therefore, it is important to get to know the influence of the PDI on the phase behavior of diblock copolymers. Many studies focused on the influence of PDI on the order–order transitions (OOTs) and order–disorder transition (ODT).[40–42] Using the SCFT model, Cooke and Shi predicted that the phase boundaries shift to smaller values of χN for polydisperse diblock copolymer melts.[41] However, this effect of polydispersity on ODT predicted by the SCFT model was not consistent with the experimental results of Lynd and Hillmyer.[43] Recently, Matsen *et al.* calculated out the phase diagram for an AB diblock copolymer melt with polydisperse A blocks and monodisperse B blocks using lattice-based Monte Carlo simulations.[42] Their results showed that the A-block polydispersity shifts the OOTs toward a higher A-monomer content. In addition, the A-block polydispersity makes the ODT move toward higher temperatures when the A blocks form the minority domains and toward lower temperatures when the A blocks form the matrix. These calculated results were in good agreement with experiments of Lynd and Hillmyer. In addition to the shift in the phase boundary, the domain spacing of nanostructures also shows dependence on the PDI.[44] Theoretical and experimental studies have both shown that an increasing PDI leads to larger domain spacing.

The above studies have improved our understanding of the self-assembly of fully flexible AB diblock copolymers. However, they did not consider the dependence of the self-assembled morphology on the chain rigidity of the copolymers. For rod–coil block copolymers, both the conformational asymmetry between the rod and coil blocks and the orientational interaction between anisotropic rod blocks can significantly change their self-assembly and lead to rich and complex nanostructures.[45–47] Various experimental and theoretical simulation studies have been performed to investigate these structures. Experiments have exhibited rich morphologies, including smectic,[48–51] arrowhead,[52] zig-zag lamellae,[52] bicontinuous[48,49,53] and cylindrical morphologies[51,53] among others. However, it is difficult to determine the local packing of rod blocks in these structures using experimental techniques. The theoretical simulation technique is a powerful method to solve this problem.[54–60] For example, using a novel SCFT lattice model, in which the rod blocks are modelled by rigid rods, An *et al.* observed several microstructures in the melts of rod–coil diblock copolymers.[54] Micellar, perforated lamellar, gyroid, and zig-zag phases have been obtained with a random initial assumption of these structures. Because there are six bond orientations in the lattice model, the orientation of rod blocks can be evaluated in the simulation. However, these six bond orientations are not sufficient to accurately simulate the packing of rod blocks. In molecular simulations, the local packing of rod blocks can be determined directly. Recently, using BD simulations with a box-size search algorithm, Glotzer and co-workers studied the morphologies and local packing of rod blocks in rod–coil diblock copolymer melts.[55] Fig. 1(b) shows four examples of morphologies found in their simulations, including monolayer and bilayer arrowhead structures, and cylindrical and wavy lamellar morphologies. The local packing of the rods within these structures was analysed. The smectic C bilayer and monolayer packing models obtained in experiments are observed in their results. Additionally, for a rod–coil diblock copolymer with long rods, the long rods tend to align parallel to each other, resulting in the formation of smectic morphologies and a zig-zag lamellar morphology. Their simulations provided deep insight into the local packing of the rod blocks within the self-assembled morphologies that should be of interest to both experimentalists and theoreticians.

Many interesting extensions to the above discussion exist that can be contemplated for the diblock copolymers as the simplest block copolymer model, such as crystallization, compressibility and chirality. One aspect that promises to be interesting is molecular chirality, occurring in every class of self-assembling materials, from liquid crystals to biological matter.[61,62] Chirality transfer from a molecule to an assembly has been observed in solution and melt assemblies.[63–68] To understand the mechanisms of mesochiral morphology formation in block copolymer melts, Zhao *et al.* recently developed an "orientational self-consistent field" theory to investigate the equilibrium phase behaviour of the melt of diblock copolymers possessing a single chiral block.[69,70] In their model, the chiral nature of the polymers is modelled as a thermodynamic preference for a cholesteric twist of the orientational order associated with the chiral block. Two mesoscopically chiral phases were observed in their simulations, including an undulated lamellar phase (UL*) and a phase of hexagonally ordered helices (H*), as shown in Fig. 1(c). Note that the experimentally observed H* morphology was predicted to be stable in the equilibrium phase diagram of chiral melts. Contrary to this SCFT study, a similar DFT simulation reported by Wang *et al.* showed that the H* morphology was metastable,[71] which is consistent with experimental observations by Ho and coworkers.[66] In the experiment, phase transitions from the H* phase to both the C phase and the G phase were found after a lengthy annealing time, suggesting that the H* phase is a long-lived metastable phase.

As mentioned above, the diblock copolymer is an ideal model to obtain a fundamental understanding of the self-assembly behaviour of block copolymers. The technological applications of block copolymers require that the block possesses the characteristics of rigidity, chirality or crystallization. For example, the block copolymers used in polymer solar cells generally contain rod or crystalline blocks.[72,73] These charac-

teristics have been shown to complicate the self-assembly behaviour of block copolymers compared with fully flexible systems, even for the simplest diblock copolymers. Among these characteristics, stiffness has been extensively studied in diblock copolymer systems. However, the phase behaviour (or phase diagram) of block copolymers with a chiral or crystalline block has rarely been reported. Understanding the phase diagram is beneficial for the design of the molecular architecture of chiral block copolymers and crystalline block copolymers to precisely control their morphology. A deeper understanding of the effects of the rigidity, chirality and crystallization on the self-assembly of diblock copolymers is desired to obtain a better performance in the technological applications of block copolymers.

3.2 ABA triblock copolymers

In addition to the AB diblock architecture, the ABA linear triblock copolymer formed by joining two identical AB diblock copolymers together by their B ends is another common block copolymer. Because the triblock copolymer is formed by joining two diblock copolymers together, the equilibrium behaviour of ABA triblock copolymers is similar to that of AB diblock copolymers.[74,75] The phase behaviour of ABA triblock copolymers is mainly dominated by L, G, C, and S, similar to that of diblock melts. Recently, the *Fddd* phase, which has been observed in AB diblock copolymers, has also been predicted as a stable structure in ABA triblock copolymers by SCFT calculations.[76]

Despite the similar phase behaviour, there still exist some notable differences in self-assembled nanostructures between ABA triblock and AB diblock copolymers. For example, the molecular architecture of the ABA triblock can lead to kinds of molecular conformations that cannot be obtained in diblock systems. These molecular conformations make a difference in the mechanical properties.[77,78] In the ABA triblock copolymer melts, the molecular conformation of each molecule can be classified as either a bridge (each A-endblock is located in a different A domain), a loop (both A-endblocks are located within the same domain), a dangle (one endblock is located in a microdomain, while the other remains in the matrix), or mixed (both endblocks are unsegregated and stay within the matrix). Extensive studies have sought to correlate the molecular conformation with bulk mechanical properties in ABA triblock copolymer melts. Early studies in these areas focused on the case of symmetric triblock copolymers. The bridging fraction for lamellar, cylindrical, and spherical morphologies was evaluated as approximately 40%–45%, 60%–65%, and 75%–80%, respectively, in SCFT calculations.[75] Recently, more studies have focused on the asymmetric A_1BA_2 triblock copolymers.[79–81] The asymmetric A_1BA_2 triblock copolymer can be progressively grown from a parent A_1B diblock copolymer. For example, Tallury *et al.* used several theoretical formalisms and simulation methods, including the SCFT, MC and DPD simulation methods, to relate molecular asymmetry to the midblock conformations and the self-assembled morphology.[81] Their results confirmed that an increase in the A_2 block length with a constant chemical composition of the parent A_1B copolymer not only introduces midblock bridging but also drives morphological transitions in these asymmetric triblock copolymers. In this class of copolymers, as in the case of symmetric triblock copolymers, a change in morphology is accompanied by a change in the bridge fraction.

Many ordered nanostructures are formed when the middle or end blocks of the ABA block copolymer become rod-like blocks.[82–84] Using the self-consistent field lattice techniques in a three-dimensional space, An *et al.* investigated the self-assembly of these block copolymer systems.[85,86] Fig. 2(a) shows the symmetric BAB coil–rod–coil and ABA rod–coil–rod

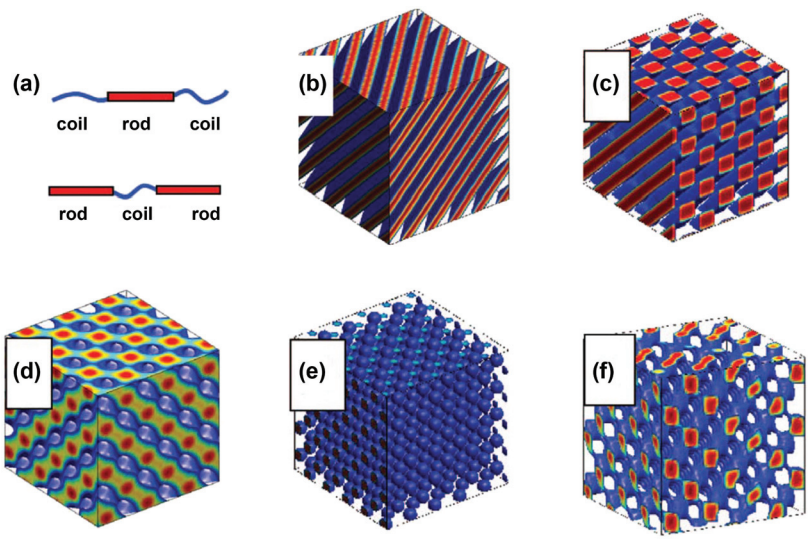

Fig. 2 (a) Molecular architecture of the BAB coil–rod–coil and ABA rod–coil–rod triblock copolymers. Lamellar (b), cylindrical (c), gyroid (d), spherical-like (e), and perforated lamellar (f) phases formed in these copolymer melts. Reproduced with permission from ref. 85, Copyright 2008, American Institute Physics, and ref. 86, Copyright 2007, American Institute Physics.

triblock copolymer models studied in their simulations. The lamellar, cylindrical, gyroid-like, spherical-like and perforated lamellae structures, as shown in Fig. 2(b)–(f), were observed both in coil–rod–coil and rod–coil–rod triblock copolymers in the SCFT calculations. The former four structures were found to be stable, while the perforated lamellae structures were metastable. These structures have also been observed in the experiment performed by Lee and coworkers.[87] They demonstrated the supramolecular structures, from 1-dimensional lamellar to 3-dimensional tetragonal superlattices, formed from coil–rod–coil molecules based on poly(propylene oxide) as coils and biphenyl oligomers as rods. Compared with coil–rod–coil BAB triblock copolymers, the free volume of ABA rod–coil–rod triblock copolymers is significantly reduced because the two end rods are coil-tethered. In addition, because of the intramolecular interactions between the two rod blocks of the same polymer chain, the rod–coil–rod prefers to adopt loops with a folded conformation, which was confirmed by Huang *et al.* using a DPD simulation.[88] Consequently, the lamellar structure of rod–coil–rod triblock copolymers is not stable for a high volume fraction of the rod component, in contrast to coil–rod–coil triblock copolymers.

According to the above discussions, compared with AB diblock copolymers, the ABA triblock copolymers show differences in their phase behaviours and self-assembled nanostructures. These differences are more marked as some blocks of the triblock copolymer become rods. Additionally, as the midblock rigidity increases, the bridge fraction conformation increases. A recent study conducted by AlSunaidi *et al.* demonstrated that the coil–rod–coil copolymers prefer to adopt the bridge conformation.[89] The presence of bridges linking separate interfaces together has been shown to strongly affect the mechanical properties of the material. Therefore, the bridging midblock of coil–rod–coil copolymers may enhance the mechanical properties of these copolymer systems. Investigations in this area can be helpful for fabricating microelectronics using rod–coil copolymers with the required mechanical properties.

3.3 ABC triblock copolymers

Given the morphological complexity of AB diblock and ABA triblock copolymers, it might be expected that the self-assembled nanostructures of ABC triblock copolymers would be even richer; indeed, this has been confirmed by recent studies. As the number of distinct blocks increases from two to three, the complexity and variety of self-assembled structures of ABC triblock copolymers are increased. Compared with AB diblock copolymers, the self-assembly behaviour of ABC triblock copolymers is dependent on more parameters because it is governed by no fewer than five parameters: two independent volume fractions, f_A and f_B, and the products $\chi_{AB}N$, $\chi_{AC}N$, and $\chi_{BC}N$ of the chain length with three different Flory–Huggins parameters. In addition, as one of the triblocks becomes a rod, the phase behaviour becomes even more complicated because of the orientational interaction between anisotropic rods. Theoretical simulations are effective and helpful in dealing with the complexity of the self-assembly behaviour of ABC triblock copolymers. In this subsection, we review recent simulation investigations of the interesting novel nanostructures formed from ABC coil–coil–coil triblock copolymers and the self-assembly behaviour of ABC rod–coil triblock copolymers.

In terms of the relative interaction strengths between three blocks, the linear ABC-terpolymers are classified into "non-frustrated" and "frustrated" cases.[90] In non-frustrated cases, the interaction strength between two endblocks is comparable to or higher than those between the neighbouring blocks. Due to the non-connectivity between the A- and C-endblocks, the A- and C-blocks are completely separated, and structures consistent with the topology of the block sequence in the linear ABC copolymer are formed. This results in the observation of core–shell versions of these microstructures in diblocks, including core–shell spheres, cylinders, gyroids, and lamellae, and alternating versions of the sphere, cylinder, and gyroid phases in which the A and C domains form alternating equivalent sublattices within a B matrix.[91–93] In addition, a novel non-cubic network nanostructure, the *Fddd* phase, has been observed in this system. This network nanostructure was first found in the non-frustrated ABC triblock copolymers created from the poly(isoprene-*b*-styrene-*b*-ethylene oxide) (ISO) system.[94–96] The *Fddd* phase was identified as one equilibrium structure, bordered by three-domain lamellae (L), a core–shell gyroid network (G), and an alternating gyroid network (G^A), as shown in Fig. 3(a). Theoretical simulations have also shown that the *Fddd* phase is a stable phase for ABC triblocks. Following the experiments of Bates *et al.*, Tyler *et al.* predicted the phase behaviour of ISO using the self-consistent field theory.[37] The phase diagram calculated by SCFT is strikingly similar to that found experimentally, as shown in Fig. 3(b). The phase diagram in Fig. 3(b) shows that the *Fddd* phase that extends to the line $f_C = 0$ is stable, implying that it must be a stable phase of AB diblock copolymer melts. Therefore, Tyler and Morse recalculated the phase diagram of AB diblock copolymer melts and found the *Fddd* network to be stable within a narrow window. Motivated by the theoretical predictions, Kim and coworkers successfully identified the *Fddd* network as one equilibrium structure in poly(styrene-*b*-isoprene) systems.[39]

In the frustrated cases, the interaction strength between two endblocks is much smaller than the interactions between other blocks; thus, the A/C contact is favoured. To minimize the area of A/B and B/C interfaces, the morphologies observed in these systems isolate the B domains into spheres, cylinders, or rings, at the expense of the formation of larger areas of the A/C interface. Eventually, a variety of novel decorated structures are formed in this case, such as spheres on spheres, spheres on cylinders, rings on cylinders, cylinders in lamellae, knitting pattern phases and helical supercylinders.[92,97,98] The interesting decorated structures were successfully predicted by theoretical simulations. For example, using a generic spectral method to solve the SCFT equations, Guo and coworkers reproduced the knitting pattern (KP) morphology.[91] The block copolymer parameters used in the calculation were chosen according to a realistic system of polystyrene-*b*-poly(ethylene-*co*-butylene)-*b*-poly(methyl methacrylate) (SEBM) triblock

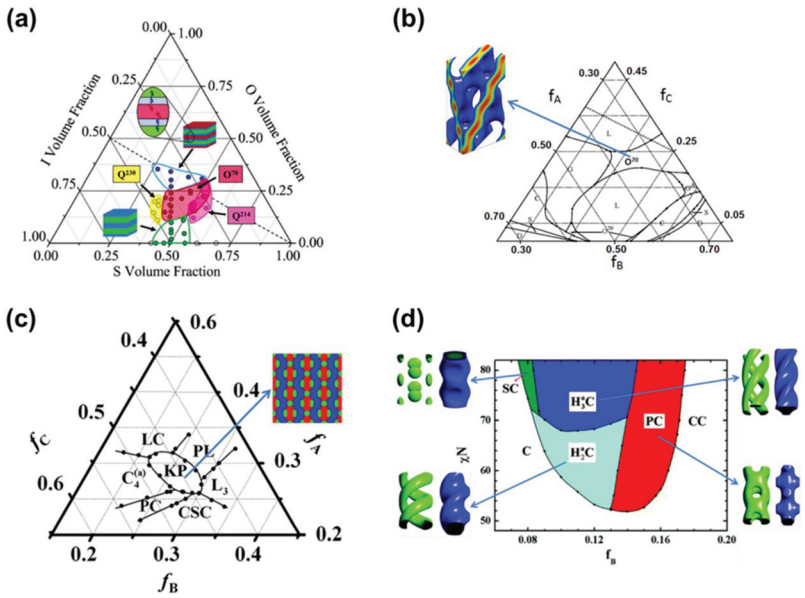

Fig. 3 (a) Phase diagram of an ISO triblock copolymer (non-frustrated) mapped out in experiments. Adapted with permission from ref. 95. Copyright 2004, American Chemical Society. (b) A partial phase triangle for a model ISO triblock copolymer calculated from SCFT. Reproduced with permission from ref. 37. Copyright 2005, American Physical Society. (c) Portion of the triangular phase diagram of a frustrated triblock copolymer with the location of the KP phase predicted by SCFT. Reproduced with permission from ref. 100. Copyright 2012, American Chemical Society. (d) Portion of the phase diagram of a frustrated triblock copolymer with the location of supercylinders predicted by SCFT. Reproduced with permission from ref. 101. Copyright 2012, American Chemical Society.

copolymers, which exhibits a fascinating two-dimensional KP phase.[99] Finally, the KP phase was predicted to occur at the parameters that mostly match the experimental conditions. However, because of the limited number of basis functions used in their approach, the accuracy of the phase boundaries obtained is limited. In order to solve this problem, Liu *et al.* applied the pseudospectral method into SCFT calculations to systematically study the stable region of the KP phase.[100] By choosing a specific set of parameters characterizing the SEBM samples, they predicted the complete stable phase region of the KP phase in the phase diagram. As shown in Fig. 3(c), in a portion of the triangular phase diagram, the KP phase is surrounded by cylinders-within-lamella (LC), perforated lamella (PL), three-color lamella (L_3), core–shell cylinder (CSC), perforated circular layer-on cylinder (PC), and quadruple cylinders-on-cylinder ($C_4^{(a)}$) phases. Comparing this predicted phase diagram of the KP phase with that constructed in experiments by Ott *et al.*,[98] they observed a small shift toward a lower composition of both A- and B-blocks. The possible reasons, which make the discrepancy inevitable, include the casting solvent, the polymer polydispersity, small composition deviations induced by experimental measurements, and uncontrollable experimental conditions. Although an inevitable discrepancy exists, the phase region of the KP phase predicted by simulations is close to the region in which the KP phase was observed experimentally.

Using the method similar to Liu and her colleagues, Li *et al.* focused on supercylindrical microstructures formed from these types of frustrated ABC triblock systems.[101] The phase diagram shown in Fig. 3(d) is constructed by a comparison of the free energies of the candidate structures. Their results indicated that in the parameter space of the calculations, the double and triple helical phases are the stable supercylindrical phases, and the phases, such as single helix-on-cylinder, rings-on-cylinder, and quadruple/triple straight cylinders-on-cylinders, are metastable. Among these structures, the experimental visualization of the double helical phase has been presented by Jinnai *et al.* in the copolymer systems of polystyrene-*b*-polybutadiene-*b*-poly(methyl methacrylate) triblock terpolymers using transmission electron microtomography,[102] which was consistent with the calculation results of Li and his colleagues.

Compared with coil–coil–coil triblock copolymers, the self-assembly of ABC rod–coil triblock copolymers is less studied for its complexity. Recently, Xia *et al.* studied the self-assembly of a linear ABC coil–coil–rod triblock copolymer melt by applying SCFT techniques.[103] In contrast to coil–coil–coil triblock copolymers that display many intricate decorated or hierarchical structures, the rod–coil triblock copolymer systems were found to exhibit seven stable self-assembly structures, including "two-colour" lamella, "three-colour" lamella, "two-colour"-perforated lamella, "three-colour"-perforated lamella, a core–shell hexagonal lattice phase, strips, and micelles, in their simulation. Among these structures, the lamellar phase was found to be stable in most of the regions of the phase diagram, especially when the length of the A and B coil blocks is equal. This phenomenon is consistent with a recent experimental study by Chang and coworkers.[104] They reported that π-conjugated rod–coil–coil triblock copolymers with vastly

different rod fractions and coil compositions exhibit a "three-colour" lamellar structure.

As noted above, a rich variety of interesting nanostructures has been produced with ABC copolymers. These nanostructures include many complex structures, such as networks, supercylinders and KP structures, most of which cannot be obtained in simple AB type block copolymers. Furthermore, because of the large parameter space of the ABC triblock copolymers, it is believed that many unknown nanostructures remain. It is a challenge to determine these nanostructures in such a large parameter space, which requires sophisticated simulation techniques and a large number of experiments.

3.4 Multiblock copolymers

It has been shown that the self-assembled nanostructures can be richer when the number of blocks increases. Therefore, multiblock copolymers that consist of many more blocks could exhibit more complicated phase behaviour and produce novel structures. The self-assembly behaviour of such copolymers has been investigated by many groups.[76,105–108] For example, the phase separation of AB multiblock copolymers was modelled by Matsen using SCFT.[76] The phase diagram of infinite linear AB multiblock copolymers predicted by SCFT is analogous to that of AB diblock copolymers. However, compared to AB diblock copolymers, multiblock copolymers have slightly larger *Fddd* regions and narrower sphere regions in the phase diagram.

In addition to AB multiblock copolymers, ABC multiblock copolymers formed by introducing a third block type can self-assemble into interesting nanostructures, including the hierarchical structures and complex mesocrystals, which have been predicted by theoretical simulations.[105,109] For example, Wang *et al.* predicted various hierarchical nanostructures, such as cylinders-in-lamella, lamellae-in-lamella, cylinders-in-cylinder and spheres-in-sphere in the melts of $A(BC)_n$ copolymers, using the method of real space SCFT.[105] In these hierarchical structures, the small-length-scale structures always remain layered, whereas the large-length-scale structures change with A-block lengths. Wang *et al.* found that the number of small-length-scale structures increases as the number of BC-blocks or the interaction strength between A and BC-blocks increases. These hierarchical structures were first observed in the experiments carried out by Matsushita *et al.* for multiblock copolymers composed of poly(2-vinylpyridine), polyisoprene and polystyrene.[110] The theoretical simulations of Wang *et al.* have successfully reproduced the hierarchical structures observed in experiments by Matsushita's group.[105]

Recently, multiblock copolymers have been demonstrated to be capable of forming complex mesocrystals. Li *et al.* applied SCFT simulations to investigate the binary mesocrystalline phases self-assembled from $B_1AB_2CB_3$ multiblock terpolymers, in which the A- and C-blocks form spherical domains.[111] Their simulations indicate that the middle B-block can be used to control the coordination number and size of the A and C spherical domains of the mesocrystalline structures. The above theoretical simulations provide compelling examples in which multiblock copolymers can be considered more likely to be a panacea than a Pandora's Box in materials design.[10] With the development of precise synthesis techniques, more complex multiblock terpolymers can be synthesized, which makes it possible to explore the theoretically predicted nanostructures by experiments.

3.5 Confined linear block copolymer systems

In addition to changing the block copolymers themselves, placing block copolymers under confinement can greatly affect the self-assembling nanostructures. New and complex nanostructures that are very different from their bulk morphologies can be formed when the block copolymers are confined on substrates introducing geometric frustration in systems.[112–114] In general, a confining environment can be characterized by its dimension (films (1D), cylindrical pores (2D) and spherical cavities (3D)), geometry (size and shape of the confining environments) and surface selectivity. Theoretical simulations have shown that the confined assembly of block copolymers is primarily dominated by the boundary selectivity and the commensurability between the size of the confining environments (D, film thickness, the diameter of cylindrical pores and spherical cavities) and the bulk period (L_0). The self-assembly of diblock copolymers under confinement in different dimensions has been extensively studied using theoretical simulations for decades.[115–120] In these studies, the effects of the commensurability condition, surface–polymer interactions, and confining geometries on the self-assembled morphologies of diblock copolymers under confinement have been discussed. Therefore, we focus on the most recent advancements in the self-assembly of copolymers under confinement, especially in the field of confined multiblock copolymers.

A large variety of nanostructures has been self-assembled from ABC triblock copolymers. Therefore, placing triblock copolymers under confinement can create even more types of nanostructures than confined simple diblock copolymers. Yu *et al.* reported an MC simulation study on the self-assembly of linear triblock copolymers under spherical confinement.[121] They focused on the self-assembled patchy nanoparticles in this system. It was observed that the number of patches increases with the increasing pore diameter. As shown in Fig. 4, with increasing pore diameter, the number of patches on a nanoparticle surface increases from one (corresponding to Janus nanoparticles) to two, four, five, six, and seven. However, when $D/L_0 > 1.9$, patchy structures no longer occur. In addition, the effects of chemical composition on the self-assembled morphologies were also investigated, and a phase diagram was constructed for confined systems with a strongly preferential wall. Despite the patchy particles, the stacked ring, lamellae and shake-hand structures were observed. Most recently, Xu and coworkers investigated the 3D confined assembly of polystyrene-*b*-polyisoprene-*b*-poly(2-vinylpyridine) ABC triblock copolymers.[122] Their experimental results confirmed the simulation predictions of Li and coworkers. In the experiments, the theoretically predicted lamella structure was observed by tailoring the interaction of the copolymer/water

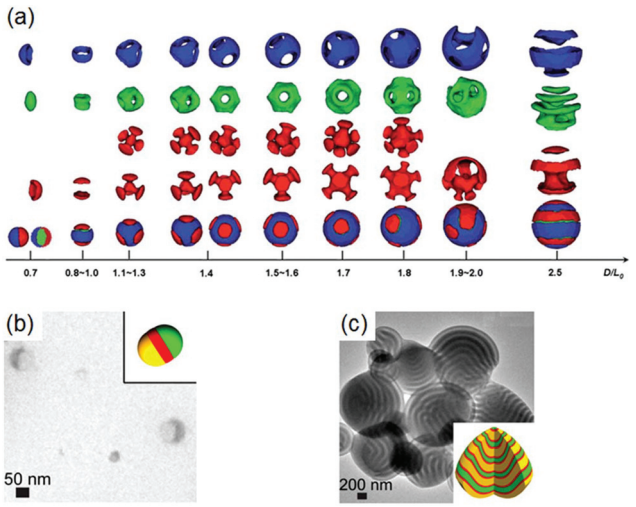

Fig. 4 (a) Self-assembled morphologies as a function of D/L_0 for triblock copolymers $A_8B_8C_8$ confined in pores. From the bottom to the top, the overall view, and the structures of the A-domain viewed from two different directions (D/L_0 = 1.1–1.8), the B-domain and C-domain are shown. Adapted with permission from ref. 121. Copyright 2014, The Royal Society of Chemistry. (b) Janus and (c) lamella structures obtained from experiments for the 3D confined assembly of polystyrene-*b*-polyisoprene-*b*-poly(2-vinylpyridine) triblock copolymers. Adapted with permission from ref. 122. Copyright 2015, American Chemical Society.

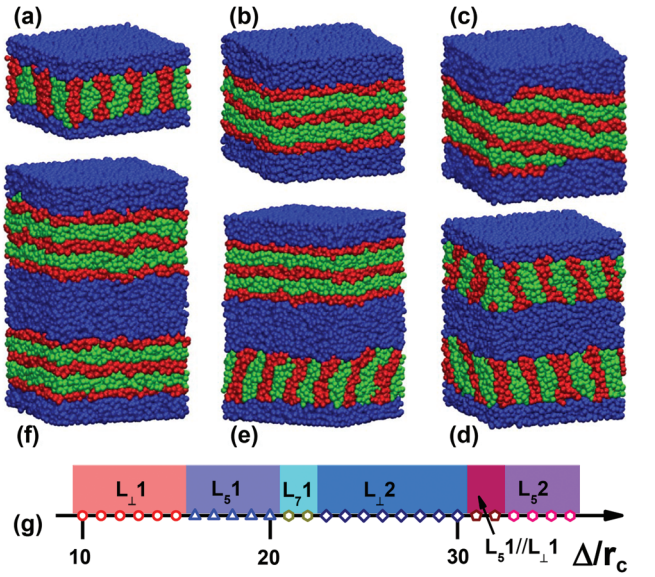

Fig. 5 Hierarchical microstructures self-assembled from $A(BC)_3$ multiblock copolymer thin films: (a) $L_\perp1$, (b) L_51, (c) L_71, (d) $L_\perp2$, (e) $L_51//L_\perp1$, and (f) L_52. (g) One-dimensional diagram for hierarchical microstructures as a function of Δ/r_c. In the representations such as L_51, the first bold letter L, subscripts, and the last number denote lamellae, the number of parallel packed small-length-scale lamellae (the symbol ⊥ means that the small-length-scale lamellae are perpendicular to the large-length-scale lamellae), and the number of the large-length-scale structures, respectively. Adapted with permission from ref. 106. Copyright 2015, American Chemical Society.

interface. Additionally, the Janus nanoparticle was also obtained under strong confinement at D/L_0 = 0.65, which is close to the size at D/L_0 = 0.7 predicted by the simulation.

Due to the complicated self-assembly behaviour, most of the studies of confined multiblock copolymers focused on low dimensional confinement. Recently, Lin *et al.* explored lamellae-in-lamellar hierarchical microstructures self-assembled from $A(BC)_n$ multiblock copolymers confined between two solid surfaces by DPD simulations.[106] They observed several hierarchical lamellae-in-lamellar microstructures, including perpendicular lamellae-in-lamella and parallel lamellae-in-lamella (see Fig. 5(a)–(f)). As shown in Fig. 5(g), as the film thickness increases, the periodicity of the large-length-scale structures increases, and the orientation of the small-length-scale structures undergoes a parallel-to-perpendicular or perpendicular-to-parallel transition. Except for the hierarchical lamellar microstructures with parallel or perpendicular arrangements of small-length-scale lamellae, the coexistence of the two small-length-scale lamellae with different orientations is also found by varying the film thickness (Δ), as shown in Fig. 5(e). There are few direct experimental studies on the controllable hierarchical microstructures of these multiblock copolymer thin film systems. As a pioneer study in the investigations of hierarchical microstructures under confinement, this simulation work can provide guidance for future studies in this area.

Copolymers self-assembling on curved surfaces (2D or 3D) are another type of multi-dimensional confined copolymer, which have received less attention than the other confined polymers. One of the main differences of nanostructures of block copolymers confined on planar (1D) and curved substrates is the nature of topological defects.[123] The curvature of the substrates imposes a topological requirement on the equilibrium structures with defects. The investigation of the defect structures and ordering kinetics of block copolymers using theoretical simulations is challenging. Recently, Zhang *et al.* used the Landau–Brazovskii theory to explore the defect structures and ordering behaviour of lamellar and cylindrical phases of diblock copolymers confined on spherical substrates.[124] For the cylindrical phase, the isolated disclinations emerge in systems with a small sphere radius. The scars are formed on the surface of a sphere with a large radius, and the number of excess dislocations in a scar is linearly proportional to the sphere radius. They observed the exponential decay of the defect fraction of the cylindrical phase. For the lamellar phase, the defect structures of hedgehog, spiral and quasi-baseball are produced on spherical substrates, and the disclination annihilation is the dominant ordering mechanism of the lamellar phase.

As mentioned above, confinement can be used to control the self-assembly of block copolymers, leading to the development of methods for engineering novel nanoscopic structures that are not available from bulk copolymers. In the application of confined copolymer systems, the annihilation of defects and the control of the orientations of the domains and mole-

cules are important issues. To obtain large-scale ordered nanostructures with defect-free morphologies and controlled orientations, directed self-assembly (DSA) is a promising method. As a special confined system, the directed self-assembly of block copolymers using chemical or topographical guiding patterns is one of the most promising applications of block copolymers.[35,125] For example, the use of elliptical nanoposts to direct the self-assembly of cylinder-forming diblock copolymers allows the generation of long-range order cylinders with a single orientation.[126] Recently, Zhang *et al.* studied the self-assembly behaviours of these types of systems using large cell simulations of SCFT.[127] Fig. 6(a) shows the schematic illustration of the template used in their simulations. By increasing the anisotropy of nanoposts (R_a/R_b) or adjusting the spacing of nanoposts (L_z/L_0), they obtained a long-range orientation order pattern in the template, as shown in Fig. 6(b)–(e). Moreover, when the spacing of elliptical nanoposts (L_z/L_0) increases slightly from 3.43 (Fig. 6(d)) to 3.60 (Fig. 6(e)), the orientation order of the cylinders increases dramatically, which indicates that the orientation order is more sensitive to the spacing of elliptical nanoposts. Their findings from the theoretical simulations are consistent with the experimental results of Ross and coworkers.[126] Ross *et al.* reported that an array of carefully spaced and shaped posts, prepared by the electron-beam patterning of an inorganic resist, could be used to template complex patterns in a cylinder-forming block copolymer. Although many studies have been conducted in this field, opportunities remain for the systematic prediction of structure formations in DSA systems.

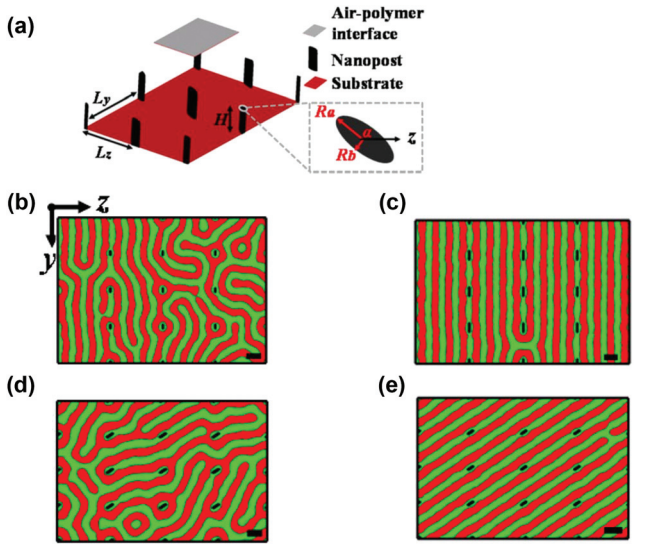

Fig. 6 (a) Schematic illustration of a template consisting of an array of elliptical nanoposts (black) between an air–polymer interface (grey) and a substrate (red). (b)–(f) Show the patterns of cylinder monolayers programmed by elliptical nanoposts: (b) and (c) with different aspect ratios of R_a/R_b = 1.6 and R_a/R_b = 3.0, respectively; (d) and (e) with different values of spacing L_z/L_0 = 3.43 and L_z/L_0 = 3.50, respectively. Adapted with permission from ref. 127. Copyright 2014, American Chemical Society.

3.6 Ordering kinetics of linear copolymers

The self-assembled structures of copolymers are not only decided by the thermodynamic properties of copolymers, but are also dependent on the control of their formation pathway. Therefore, understanding the formation kinetics of nanostructures self-assembled from block copolymers is helpful in designing suitable processing routes to obtain specific ordered structures. Extensive studies on the ordering kinetics of copolymer systems have shown that microphase separations can occur *via* two possible mechanisms: spinodal decomposition and nucleation growth. Depending on the magnitude of the driving force under the given conditions, one of the two mechanisms is preferred. The nucleation and growth mechanism is preferred when the system is in the metastable region, and spinodal decomposition is the dominant mechanism in the unstable region.[128] Theoretical simulations are helpful for gaining insight into the formation kinetics of ordered structures formed by block copolymers. In this subsection, we focus on the ordering kinetics of diblock copolymer and triblock copolymer systems.

The kinetics of phase separation in diblock copolymers has been extensively studied. It has been shown that S, C, G, and L morphologies can be obtained by the appropriate selection of ordering temperature and copolymer composition.[129] Recently, most simulation investigations of the formation kinetics of diblock copolymers focused on the nucleation of ordered phases, which is the frequent process during the order–order transition (OOT).[130–132] Cheng *et al.* utilized the SCFT to study the nucleation of various ordered phases in diblock copolymers by examining the minimum energy path.[133] During the G → C transition, the fracture of the gyroids and the reconnection were propagated throughout the material, whereas the emergence of gyroids from cylinders was shown to proceed through the distortion, disconnection, and reconnection of the cylinders. These morphological structures involving gyroid–cylinder transitions were found to be consistent with experiments by Park and coworkers.[130] In addition, by comparing the free-energy barrier of the minimum energy path, they found that the L → HPL (hexagonal perforated lamellae) → G path was preferred within the L → G transition. This prediction provides an explanation for the prevalence of the HPL in gyroid-forming block copolymers observed experimentally.[134,135]

The ordering kinetics of triblock copolymers is more complicated than that in diblock copolymers. Studies in this area focused on the order of the separations between A, B and C blocks. During the ordering processes for ABC linear triblocks, the order of the separations between A, B and C blocks is dependent on the chemical composition and interaction parameters.[136–138] The microphase ordering processes for ABC triblock copolymers can be through a one-step or two-step mechanism (Fig. 7). In the one-step mechanism M_I, the three species segregate simultaneously after the system is quenched from a disordered state, and in the two-step mechanism M_{II}, which is classified into three subtypes: in M_{IIA}, M_{IIB} and M_{IIC},

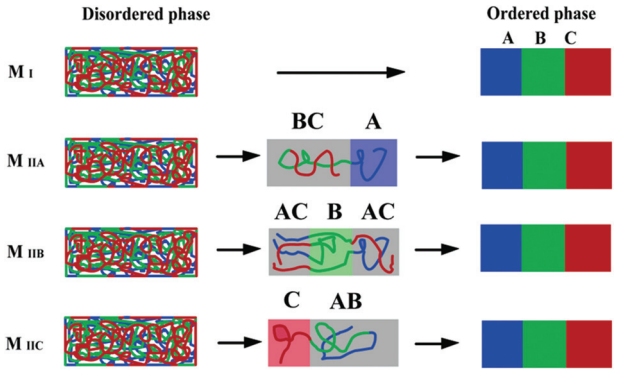

Fig. 7 Schematic illustration of possible ordering mechanisms for the disorder-to-order transition in linear ABC triblock copolymer melts. M_I is for the one-step ordering mechanism. M_{IIA}, M_{IIB} and M_{IIC} are for the two-step ordering mechanisms. Adapted with permission from ref. 139. Copyright 2005, American Chemical Society.

one block of the triblock (A, B or C) separates from the other two blocks first, followed by segregation from the remaining two blocks. The ordering process depends on the compositions and the interaction energies among the three species. Using a dynamic DFT simulation, Xia *et al.* obtained the time evolution of the phase structures of triblock copolymers.[139] Their results revealed that when the chain length of one species dominates the other two, the phase ordering always proceeds through a two-step mechanism with the longest one segregating at first, resulting in the formation of a three-phase morphology at the end. When the chain lengths of the three species are comparable, the ordering mechanism depends on the strength of the interaction parameters: in the case of symmetric interaction, the microphase separation occurs through a one-step mechanism, while for the asymmetric interaction case, it occurs through a two-step mechanism with the most incompatible species segregating at first.

Theoretical simulations have significantly enhanced our understanding of the kinetics of morphological transitions. However, there are many interesting problems or challenges remaining. For example, it is complicated to determine the formation kinetics of novel complex nanostructures, such as the supercylindrical structures, hierarchical structures and mesocrystals, which are mentioned above. Recently, Lin *et al.* studied the formation dynamics of the hierarchical microstructure of the lamellar-in-lamellar formation using DPD.[106] They found that the large-length-scale structures were first formed and then the small-length-scale structures were adjusted to accommodate the large-length-scale structures. Their finding reveals that the formation of small-length-scale structures always lags behind that of large-length-scale structures, which is helpful in the understanding of the ordering kinetics of hierarchical structures. However, additional investigations are required on the formation kinetics of these complex nanostructures for their successful fabrication.

4. Self-assembly of graft copolymers

The molecular architecture has been shown to be an important factor in determining the morphologies of the microstructures, phase behaviours, and material properties. Graft copolymers, which consist of a long backbone block and several side chains, exhibit more intricate self-assembly behaviours compared to the above linear block copolymer systems. Most of the research has focused on the graft copolymers due to their unique material properties and technological applications.[140,141] In this section, we feature the nanostructures self-assembled from AB graft and ABC graft copolymers.

4.1 A-*g*-B graft copolymers

The phase behaviour of diblock copolymers is determined by the interaction parameters and the composition fraction. For A-*g*-B graft copolymers, in addition to these two parameters, the architectural parameters (graft number, junction distribution, and the number of arms per junction) exert a significant effect on the phase boundaries and stability regions of the phase diagrams. Specially, graft copolymers can be designed into a comb-shaped supramolecular architecture or a comb-coil block copolymer, which have been shown to have the ability to self-assemble into novel hierarchical structures. In this subsection, we review the effect of architecture on the phase behaviour and nanostructures of graft copolymers and the novel hierarchical structures self-assembled from comb-coil block copolymers.

Recently, to systemically examine the phase behaviour of graft copolymers, Lin and coworkers performed systemic work on the self-assembly of A-*g*-B graft copolymers using a reciprocal-space SCFT.[142,143] Fig. 8(a) shows the molecular architecture of the A-*g*-B graft copolymer studied in their simulations. There are L, G, C, and S phases in the phase diagrams of A-*g*-B copolymers, which are illustrated in Fig. 8(b)–(d). Because of the asymmetry in the molecular architecture, compared with linear diblock copolymers, graft copolymers present asymmetric phase diagrams. In addition, the self-assembly behaviour of graft copolymer melts strongly depends on the first junction position (τ_1), the graft number (z) and the number of arms per junction (p). As shown in Fig. 8(b)–(d), when τ_1, z or p increases, corresponding to a lateral crowding of the graft arms, the OOT lines shift to a higher backbone composition f_A. This behaviour can be rationalized by considering the stretching energy of the chains, which changes with the variation of architectural parameters. In an incompressible system, the crowding of the graft arms results in a higher stretching energy. To alleviate this effect and to lower the overall free energy, the interface curves away from the stretched graft arm domain, resulting in a preference for graft arms to reside on the convex side of the interface. These theoretical findings are consistent with the experimental studies of Gido and coworkers.[144–146] Gido *et al.* synthesized a series of well-defined graft copolymers with a polyisoprene (PI) backbone and polystyrene (PS) branches (PS-*g*-PI). By exerting precise control over the backbone molecular weight, the arm

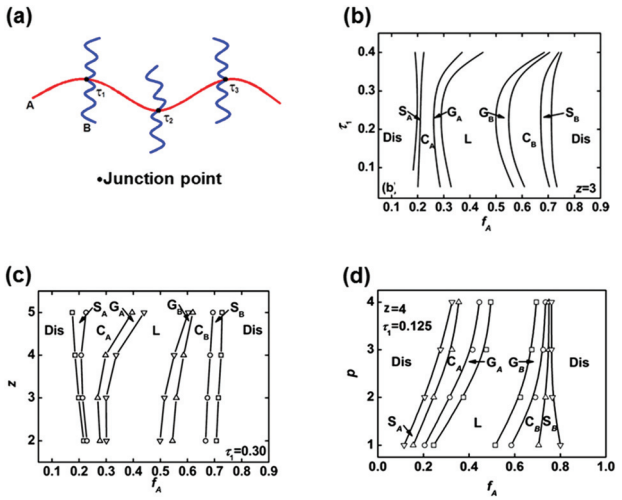

Fig. 8 (a) Molecular architecture of the multigraft copolymer with the number of graft arms per junction p = 2 and the number of junctions z = 3. (b) Mean-field phase diagrams in $\tau_1 - f_A$ space for graft copolymers with z = 3. (c) Mean-field phase diagram in $z - f_A$ space for graft copolymers with τ_1 = 0.30. (d) Phase diagrams in $p - f_A$ space for AB multigraft copolymers. (a) and (d) Adapted with permission from ref. 142. Copyright 2008, American Institute of Physics. (b) and (c) Adapted with permission from ref. 143. Copyright 2008, American Chemical Society.

molecular weight, the arm polydispersity, and the placement of junction points, they obtained classical microdomain geometries of lamellae, cylinders, and spheres in these experimental studies.

While the junctions along the backbone are constrained to the domain interfaces, the backbone blocks of graft copolymers can take either a loop conformation whose neighbouring junctions are located in the same domain or a bridge conformation whose neighbouring junctions are anchored on different domain interfaces. The bridge conformation can also enhance the mechanical performance of graft copolymers, as do linear block copolymers.[146,147] To understand the structure–property relationship, Lin *et al.* studied the bridging properties of graft copolymers using a real space algorithm of the self-consistent field theory in two dimensions.[148] Their studies focused on cylindrical and lamellar structures. In both structures, the bridge fraction showed a tendency to decrease, as the length of free end blocks and the number of branches increased. In addition, the bridge fraction of the lamellar phase was found to be lower than the cylindrical phase. The position of graft points and the number of branches that influence the bridge fraction are two important parameters for material design.

As a special type of graft copolymer, the comb-coil block copolymers are expected to produce hierarchical structures. Pioneering studies by ten Brinke *et al.* and Wang *et al.* based on random-phase approximation analysis showed that these graft copolymers can exhibit unusual phase behaviours.[142,149,150] The A-coil blocks and comb blocks would first be separated, instead of the separations between the backbone and grafts, which indicates that if the comb blocks can be further microphase separated, the two-component coil-comb block copolymers can form hierarchical structures. Based on this consideration, Wang *et al.* performed an SCFT study on such coil-comb block copolymers.[151] It was found that when the interaction strengths are high enough, the coil-comb block copolymers could self-assemble into hierarchical structures, such as lamellae-in-lamella. In these structures, the separation between the coil and comb blocks produces the large-length-scale structures, whereas the separation in comb blocks generates the small-length-scale structures. It was revealed that the parallel lamellae-in-lamella could be transformed into perpendicular lamellae-in-lamella when the interaction strength is relatively high. This transformation can be ascribed to the optimization of the internal energy. Compared to the parallel structures, the interactions between continuous A-backbone and B grafts can be effectively avoided in the perpendicular structures.

The nanostructures, phase transitions and conformational variations of graft copolymers can also be affected by the rigidity of polymer backbones or side chains. Related experiments showed that the rod backbone plays an important role in the functional properties and the stacking structure of graft copolymers. For example, most recently, Lee *et al.* produced the self-assembled nanostructures of rod–coil A-*g*-B graft copolymer systems created from poly(fluorene-*alt*-phenylene)-*g*-poly (2-vinylpyridine) (PFP-*g*-P2VP).[4] Ordered structures, such as cylinders and lamellae, have been observed in their experiments and SCFT simulations, respectively. In addition, by using the controlled nanostructures of PFP-*g*-P2VP and the strong emitting properties of the backbone, they successfully developed multicoloured colloidal particles that emit a broad range colour spectrum from blue, white, to orange light. Such a combination of theoretical simulations and experimental observations could be performed more frequently to understand and control the nanostructures formed in copolymer systems.

4.2 ABC graft copolymers

With the introduction of a third block into the graft copolymers, more complex architectures are formed, such as A_{m+1}-*g*-(B-*b*-C)$_m$, A-*b*-(B-*g*-C) and ABC π-shaped graft copolymers. The parameter space of the ABC graft copolymers is so large that it is difficult to investigate the self-assembly behaviour by experiments. Many interesting nanostructures formed by these complex copolymers have been observed in theoretical simulations. Moreover, while the backbone or the side chain block becomes rod block, the self-assembly behaviour becomes more complicated. The various architectures of the ABC graft copolymers provide their enormous applications in the fabrication of functional devices and materials; thus, it is important to get to know the correlation of various architectures with the self-assembled structures. Recent simulations of ABC graft copolymers are demonstrated in this subsection.

Considering the complex architectures of comb block copolymers composed of main chain and side chains segments,

Wang *et al.* systematically investigated the self-assembly behaviours of $A_{m+1}(BC)_m$ graft copolymers through SCFT.[152,153] Eight stable ordered morphologies were observed: a two-colour lamellar phase (LAM2), three-colour lamellar phase (LAM3), hexagonal lattice phase (HEX), core shell hexagonal lattice phase (CSH), two interpenetrating tetragonal lattices (TET2), a core shell tetragonal lattice (CST), a lamellar phase with beads inside (LAM + BD), and a lamellar phase with alternating beads (LAM + AB), as shown in Fig. 9. They constructed phase diagrams of $A_{m+1}(BC)_m$ copolymers with various numbers of side chains (m) with different interaction parameters. By a comparison of these phase diagrams of $A_{m+1}(BC)_m$, they found that the disordered phase easily forms when the comb copolymer has the longer main chain A or longer side chain with a short block C, *i.e.*, a longer block B. The simulated results provided a suitable reference for the design of functional materials with complex architectures.

As a type of comb-coil block copolymer, A-*b*-(B-*g*-C) graft copolymers can also self-assemble into hierarchical structures. The self-assembly of A-*b*-(B-*g*-C) graft copolymers has been studied by Huang *et al.* using DPD simulation.[154,155] By varying the block composition, the interaction parameter and the side chain number, they observed a variety of nanostructures, including hierarchical structures. Both the immiscibility degrees between B and C and those between the A-coil block and the BC-comb block are significant for the formation of the small-length-scale segregated lamellae within the large-length-scale structures. If the three components are significantly incompatible with one another, then various experimentally observed structures-within-structures, such as spheres-within-lamellae, cylinders-within-lamellae, gyroids-within-lamellae, lamellae-within-lamellae, lamellae-within-cylinders, and lamellae-within-spheres, were obtained in the simulations.

When the side chains grafted on the polymer backbone of graft copolymers become rigid segments, side chain liquid crystalline (SCLC) block copolymers are obtained. In contrast to the morphologies exhibited by rod–coil linear block copolymers, side-chain liquid crystalline block copolymers exhibit richer self-assembly characteristics that manifest in an interplay between the backbone blocks of copolymer ordering and liquid crystalline ordering between rod side chains.[156–159] Recently, Li *et al.* performed a DPD simulation to study the phase behaviours of SCLC block copolymers, which consist of flexible A blocks and flexible B blocks grafted by rigid C side chains.[160] Fig. 10(a) shows the coarse-grained model of the graft copolymer investigated in the simulations. Various classical mesophases, such as spheres (S_A), cylinders (C_A), gyroids (G_A and G_C), and lamellae (L), were formed, as shown in Fig. 10(b)–(f). The subscripts A and C in S, C, and G indicate that the minor domains of the ordered structures are formed by A and C blocks, respectively. The nanostructures

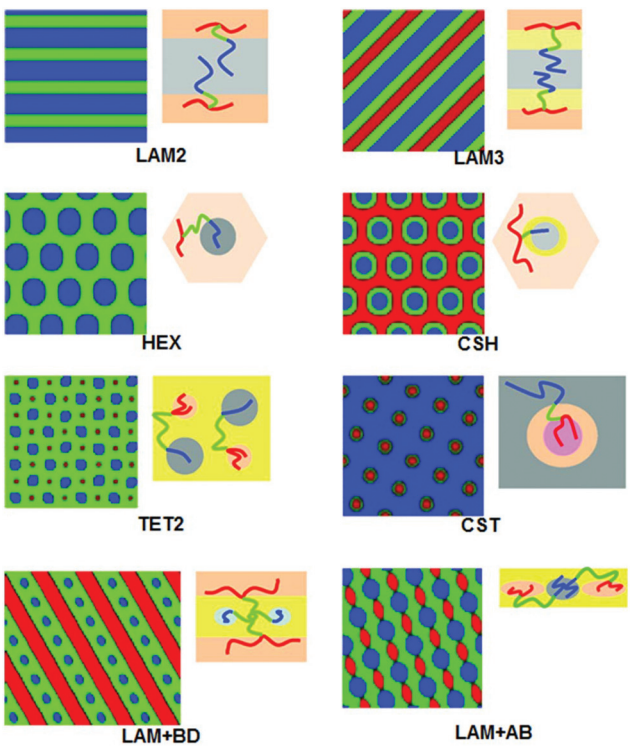

Fig. 9 Ordered morphologies for $A_{m+1}(BC)_m$ comb block copolymers, m = 1, 2, 3. The chain packing information of the eight morphologies is also presented on the right side of the morphology, correspondingly by taking $A_2(BC)$ as an example. Adapted with permission from ref. 152. Copyright 2009, American Chemical Society.

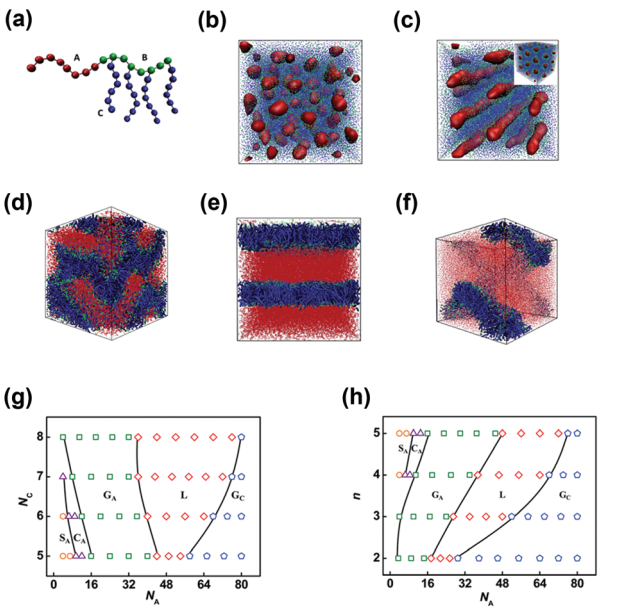

Fig. 10 (a) Coarse-grained model for the SCLC block copolymers. A and B blocks are flexible, and C block is rigid. (b)–(f) Ordered structures, S_A, C_A, G_A, L and G_C, formed by SCLC block copolymers. (g) Phase stability regions of SCLC block copolymers in the space of N_C *vs.* N_A for SCLC block copolymers with N_B = 8 and graft number n = 4. (h) Phase stability regions in the space of graft number n *vs.* N_A for SCLC block copolymers with N_C = 6. Adapted with permission from ref. 160. Copyright 2015, Royal Society of Chemistry.

self-assembled from the SCLC copolymers can be controlled by A and C block lengths (N_A and N_C) and the graft number (n). As shown in Fig. 10(g) and (h), the S_A, C_A, G_A, L, and G_C phases are formed sequentially as the A block length increases. In addition, as the C block length or graft number increases, the regions occupied by the G_A and L phases become wider, indicating that the SCLC block copolymers tend to form G_A and L phases at higher N_C and n. The lamellar phases of SCLC copolymers have also been observed in experiments by Yamada and coworkers.[161] In the experiments, the side chain LC segments formed the smectic A crystalline phase and isotropic arrangements with an increase in temperature. This tendency coincides well with the simulation results of Li and his coworkers.

Generally, the domain sizes of nanostructures self-assembled from linear block copolymers are limited to less than 100 nm. Graft copolymers with a polymeric backbone and dense side chains can produce ordered arrays with domain sizes larger than 100 nm. For example, bottlebrush polymers, a special graft copolymer, with one or more polymeric side-chains attached to each repeating unit of a linear polymer backbone, have been shown to segregate into large domain sizes.[162] This field is exciting because the self-assembly of graft copolymers in the solid state with a large domain size offers an attractive method to form optical materials. Indeed, many groups have reported the selective reflection of blue or green light in bottlebrush block copolymer films and melts. For example, Sveinbjörnsson *et al.* successfully prepared nanostructures self-assembled from a series of PS–PLA bottlebrush block copolymers with photonic bandgaps spanning the entire visible spectrum, from ultraviolet to near infrared.[163] The optical properties are influenced by the microdomain structures (*e.g.*, cylindrical, lamellar, *etc.*), which are primarily determined by the molecular architecture. However, the influence of the molecular architecture on the self-assembly behaviour of these copolymers has only been reported for a few systems.[164,165] It is necessary to perform more detailed studies including theoretical simulation studies to improve our understanding of the influence of the backbone and side chain length, as well as the composition of the copolymer on the morphologies and domain sizes.

Theoretical simulations have significantly enhanced our understanding of the self-assembly behaviour of graft copolymers. Rich morphologies have been observed for these copolymers. However, problems and opportunities remain in this field. For example, placing graft copolymer systems under confinement can greatly affect the self-assembled nanostructures. However, the self-assembly of confined graft copolymers has received less attention because it is more complicated than that in linear block copolymers.

In addition, the formation kinetics of the self-assembled nanostructures in graft copolymers is so complex that it has only been marginally explored to date. From the significant difference between the ordering process of diblock and triblock copolymers, it can be inferred that the molecular architecture could play important roles in the ordering process of graft copolymers. Systematic investigations of the self-assembly of confined graft copolymers and the ordering process of graft copolymers are required in facilitating the technological applications.

5. Self-assembly of complex copolymers

5.1 Copolymers with a complex architecture

The topology of the copolymers plays a crucial role in determining the final nanostructures. In addition to the linear arrangement, copolymer blocks can also be arranged into star-like or dendritic architectures. This inspires the work of theoretical simulations on the effect of these complex architectures on the self-assembly behaviour, which is featured in this subsection.

5.1.1 Star copolymers. Because the incompatible component polymer chains are tethered at a junction point, the star-shaped block copolymers are in a very frustrated state in bulk. Their junction points cannot be aligned on two-dimensional planes but can be aligned on one-dimensional lines. Compared to linear block copolymers, an additional entropic effect due to the junction constraint of the centre cores arises in the star block copolymers. The existence of the cores becomes a strong topological constraint that regulates the formation of various geometric structures, mostly with polymer–polymer interfaces without junctions. In this subsection, we review the nanostructures self-assembled from ABC star terpolymers, both in bulk and under confinement. The formation kinetics of these nanostructures is also demonstrated.

There are a number of nanostructures self-assembled from ABC star copolymers. Recently, to explore the rich phase behaviours of these copolymers, Xu *et al.* developed a two-step strategy within the framework of the SCFT using a combination of fast algorithms and novel initialization procedures.[166] Using the proposed strategy, ten stable phases were observed in their simulations. Four of them are shown in Fig. 11, including cylinder-in-lamellae with perpendicularly oriented cylinders and 2D tilting patterns ([6.6.6], [8.8.4], and [3 3 4 3 4]). In the tilting patterns of [*k.l.m*....], the integers indicate that the *k*-gon, *l*-gon, *m*-gon, *etc.*, meet consecutively at each vertex. Xu and coworkers presented a phase diagram of symmetrically interacting ABC star triblock copolymers with fixed Flory–Huggins parameters and found that in the centre of the phase diagram, the arm lengths were comparable, and the stable phase was the 2D tilting pattern. This finding is consistent with the results of 2D SCFT calculations and an MC simulation.[167,168] Furthermore, these simulation results conformed with the experimental observations of Matsushita's group, who reported a variety of tilting pattern structures and hierarchical structures in the ABC star copolymers composed of polyisoprene, polystyrene and poly(2-vinylpyridine).[169–173] As can be seen in Fig. 11, the nanostructures obtained in theoretical simulations are well consistent with the experimental results. Most recently, Jiang *et al.* extended the related studies to the

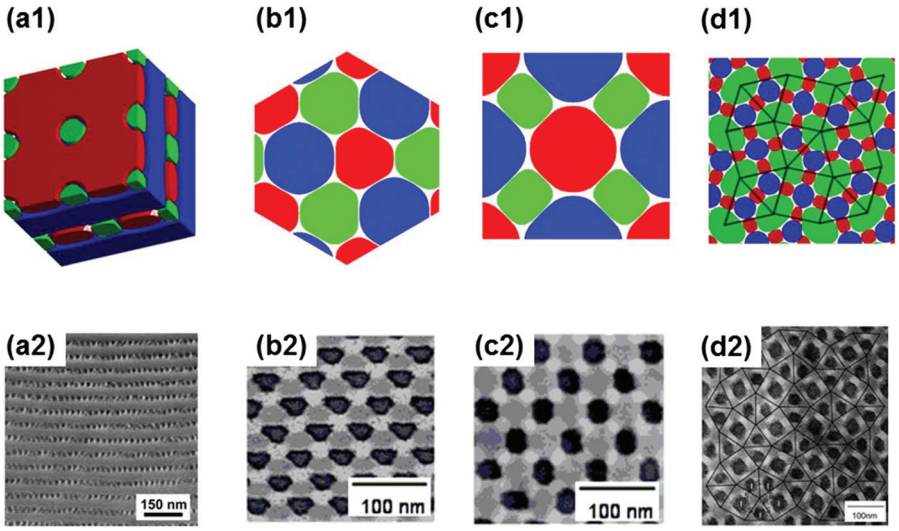

Fig. 11 Stable phases of (a) hierarchical cylinder-in-lamellae, (b) [6.6.6], (c) [8.8.4] and (d) [3 3 4 3 4] tilting structures obtained from (1) SCET calculations and (2) experiments. The experimental samples are star-shaped copolymers created from polyisoprene, polystyrene, and poly(2-vinylpyridine). Adapted with permission from ref. 166, 169 and 173. Copyright 2013, 2007 and 2004, American Chemical Society. (d2) Adapted with permission from ref. 170. Copyright 2005, Wiley-VCH.

asymmetrically interacting ABC star triblock copolymer melts.[174] They summarized their simulation results into a triangular phase diagram. The centre region of the phase diagram is occupied by 2D tilting patterns, while lamella-, cylinder-, sphere-, and gyroid-based structures are near the corner of the triangular phase diagram. This phase behaviour is highly similar to that of symmetrically interacting star terpolymers, which indicates that the nanostructures obtained from the ABC star terpolymers are less sensitive to the relative interaction strengths.

Placing the ABC star copolymers under confinement can create new phases that cannot be found in bulk. In contrast to well-studied confined diblock copolymers, fewer studies have been conducted on confined ABC star triblock copolymers. Early simulations were concentrated on the phase behaviour of ABC star triblock copolymers confined under thin films. By varying the film thickness and the strength of the surface fields, Yang *et al.* identified a variety of morphologies and evaluated the phase behaviour of ABC star triblock copolymers using SCFT simulations.[175] The volume fraction of three different polymer species was chosen to be near-symmetric in their model. In the parameter space they explored, they only obtained cylinder phases in the bulk system of ABC star copolymers. In contrast to the bulk self-assembly, self-assembly under the confinement of thin films makes these copolymers exhibit more nanostructures, including cylinders, perforated lamellae and lamellae, and other complex hybrid structures. Some of them involve novel structures, such as spheres in a continuous matrix and cylinders with alternating helical structures, which were found to be stable with a suitable film thickness and surface field. However, under the confinement of thin films, the formation of new phases from ABC star triblock copolymers is limited. Numerous novel nanostructures can be generated in ABC star triblock copolymer systems confined in pores and spherical cavities. For example, helix-based structures have been predicted in ABC star triblock copolymers inside a pore with a neutral surface by Liu *et al.* using SCFT.[176] In their SCFT calculations, they focused on the ABC star terpolymer, which forms hexagonally arranged segmented cylinders in the bulk. As the pore size increased, the phase sequence from single-cylinder, to single-helix, and then to double-helix was observed. Most recently, Li *et al.* observed groups of sphere centric structures, such as ring-like and lamellae-like structures, self-assembled from these copolymers in a spherical cavity using SCFT.[177] The theoretical predictions in these studies provide guidance for the practical fabrication of useful nanostructural materials.

The formation mechanisms of nanostructures of ABC star terpolymers are more complicated than those of linear block copolymers. Recently, Lin *et al.* have investigated the formation kinetics of nanostructures self-assembled from ABC star block copolymers with symmetric interaction parameters, using a theoretical approach coupling the dynamic SCFT and variable cell shape (VCS) method.[178] As the star copolymer melts are quenched from the disordered states to the ordered states, three types of ordering mechanisms are discovered in their simulation (Fig. 12). When the lengths of two arms are longer than that of the third arm (Fig. 12a), the two long arms are quickly segregated from each other and the short arm is slowly separated from the formed domains. When the lengths of the three arms are comparable (Fig. 12b), the three arms are simultaneously segregated from each other. When one of the arms is long (Fig. 12c), the longer arms are separated from the shorter mixed domains, following the further de-mixing of the shorter arms.

5.1.2 Dendritic copolymer. Dendritic copolymers, including dendrimers and hyperbranched copolymers, also exhibit

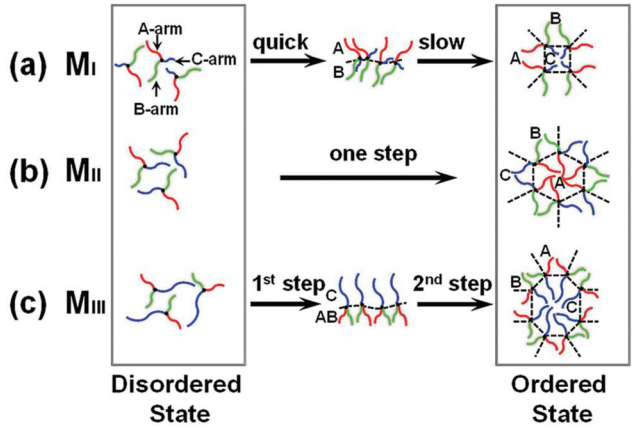

Fig. 12 A schematic illustration of the ordering mechanisms for the disorder-to-order transition of the ABC star terpolymer melts. (a) Ordering mechanism M_I for terpolymers when the lengths of two arms are longer than that of the third arm. (b) Ordering mechanism M_{II} for terpolymers when the length of the three arms is comparable. (c) Ordering mechanism M_{III} for terpolymers when the lengths of two arms are shorter than that of the third arm. Adapted with permission from ref. 178. Copyright 2014, Royal Society of Chemistry.

unusual morphologies, which include complicated three dimensional nanostructures such as quasicrystallines.[179–181] Grason *et al.* investigated the phase behavior of AB-type copolymer melts with multiple branches (A is the first generation block and B is the branched block) using SCFT.[182] Their results showed that, compared to the predicted phase behavior of linear AB block copolymer melts, the phase boundaries of these branched copolymer melts moved systematically towards larger values of the volume fraction of B blocks. In addition, a novel nanostructure of the cubic phase of spherical micelles (A15 phase) which is absent in linear diblock polymer melts, was observed in AB-type copolymers melts with multiple branches in the theoretical simulation.

Using a similar approach which Grason used above, Fredrickson *et al.* studied the self-assembled nanostructures of two different ABC-type pitchfork-like dendritic copolymer melts.[183] These copolymers which they investigated consist of three distinct blocks that correspond roughly to the handle, the connecting middle dendron structure, and the attached tines of a pitchfork. They considered two molecular structures of such a dendritic copolymer: the first one consists of a copolymer that has a simple Y-junction middle block which connects the handle to two tines, and the second is similar to the first except its dendritic middle block branches twice to connect to four tines. Several morphologies including lamellae, columnar square, rectangular and hexagonally packed structures were observed by varying the architectures and lengths of the blocks as well as their incompatibilities in the simulation. Among these structures, they have focused on the stable regions of columnar square and rectangular packed structures. Their results indicate that, for both molecular structures of the pitchfork-like dendritic copolymer, a certain fraction of the middle dendritic structure is essential for stabilizing these two structures. In addition, this middle dendron must be relatively compatible with the handle.

With the development of synthetic technology, more block copolymers with complex architectures such as star copolymers with more arms, ring copolymers, H-shaped and π-shaped copolymers are available.[144,184,185] These complex architectures enrich copolymer systems with novel nanostructures. Theoretical simulations have predicted some of these structures. For example, Sun *et al.* applied SCFT to study the self-assembled structures of π-shaped ABC block copolymers.[186] Various nanostructures such as the lamellar phase, lamellae with beads inside and structures with tilting patterns were predicted. Sun *et al.* also extended their SCFT calculations to the self-assembly behaviour of H-shaped block copolymers.[187] In the melts of H-shaped block copolymers, they found four different morphologies including the lamellar phase, hexagonal lattice phase, core–shell hexagonal lattice phase, and two interpenetrating tetragonal lattices. These simulation results may help the design and the synthesis of block copolymers with different microstructures. However, the above studies are concentrated in a limited parameter space. Systemic investigations of block copolymers with complex architectures are required for deeply understanding the self-assembly behaviour.

5.2 Copolymer blends

In addition to neat copolymer melts, the addition of homopolymers into copolymers or the blending of two or more copolymers with distinct molecular weights or compositions is another strategy to achieve the desired morphologies. However, it is complicated to investigate the thermodynamic stability and formation kinetics of self-assembled structures in mixture systems. In this regard, theoretical simulations offer efficient and economical methods to study the self-assembly behaviours of mixture systems. In this subsection, we first represent simulation investigations on the effect of the addition of homopolymers on the nanostructures of blends of copolymer melts. Then, recent studies using theoretical simulations on the self-assembly of blends of copolymers with supramolecular interactions are discussed.

Many studies have shown that the addition of homopolymers to a copolymer melt swells and stabilizes the ordered microstructure.[188] Thus, the pattern dimensions of the ordered structures can be fine-tuned through the addition of homopolymers with different molecular weights. For example, de Pablo *et al.* studied the effect of the length and amount of homopolymers on the self-assembly of mixtures of AB-diblock copolymers with the corresponding A and B homopolymers using a coarse grain Monte-Carlo simulation.[189] They studied the lamellar spacing by varying the molecular weight and the amount of homopolymers. The molecular weight was found to influence the domain size. The addition of a homopolymer with a higher molecular weight produced a greater domain size. These simulation results are consistent with the experimental results. For example, Yang *et al.* reported that the domain size of poly(styrene-*b*-dimethylsiloxane) showed an

obvious increase with the increasing molecular weight of the additional homo-polystyrene.[190]

The introduction of supramolecular interactions, such as hydrogen bonds and ligands, into the blend system would effectively suppress the macrophase separation and encourage the self-assembly of molecules into hierarchical nanostructures.[191–193] The self-assembly of AB diblock copolymer/C homopolymer blends with reversible supramolecular interactions is a suitable method to obtain these nanostructures. Using the real-space self-consistent field theory, Zhuang *et al.* investigated the self-assembly of these block copolymer/homopolymer blends.[194] In their simulations, a reversible bond is formed between the B free end of the AB diblock copolymers and one end of the C homopolymers; therefore, the supramolecular blends consist of the AB diblock copolymers, C homopolymers, and supramolecular ABC terpolymers. The volume fraction of these three constituent polymers is dependent on the bonding strength ($h/\chi N$) and the blend ratio. This leads to the dependence of the self-assembled hierarchical nanostructures on the total C volume fractions and bonding strength, as shown in Fig. 13. At a weaker bonding strength ($h/\chi N$ = 0.14, Fig. 13a), the hierarchical nanostructures, including spheres-in-cylinders (Fig. 13a (1–3)) and cylinders-in-lamellae (Fig. 13a(4)), are observed. When the bonding strength is stronger ($h/\chi N$ = 0.3, Fig. 13c), as the total C volume fraction increases, the nanostructures transform from cylinders to lamellae. Overall, the hierarchical structures tend to appear in the region of weak bonding strength. In addition, an increase in the C homopolymer volume fraction or the bonding strength leads to the formation of lamella structures.

The blends of AB- and B′C-diblock copolymers with B- and B′-blocks miscible *via* hydrogen-bonding interactions are also a widely-studied system. Most recently, Zhang *et al.* extended SCFT with hydrogen-bonding interactions described by the Yukawa potential to study this system.[195] In this work, they assumed that the hydrogen-bonding interactions are electrostatic dipole–dipole interactions. The dipole–dipole interactions were described by Yukawa potentials, which are also named screened Coulomb potentials. This approach can overcome the deficiencies of commonly used methods; it could rationally describe the immiscibility between different polymers and could be suitable for multiple-hydrogen-bond supramolecular systems. The systems were found to self-assemble into parallel lamellae-in-lamellae and perpendicular lamellae-in-lamellae nanostructures. They indicated that the appearance of parallel/perpendicular lamellae-in-lamellae structures was dependent on the strength of the hydrogen-bonding interactions related to the density of hydrogen bonds and the characteristic lengths of the Yukawa potentials. The perpendicular lamellae-in-lamellae structures were stable with strong hydrogen-bonding interactions. In addition, they successfully showed that an increase in the hydrogen-bonding interactions could lead to a phase transition from tetragonal to hexagonal cylinders, which was observed in experiments for which the mechanism is not yet well understood.[196]

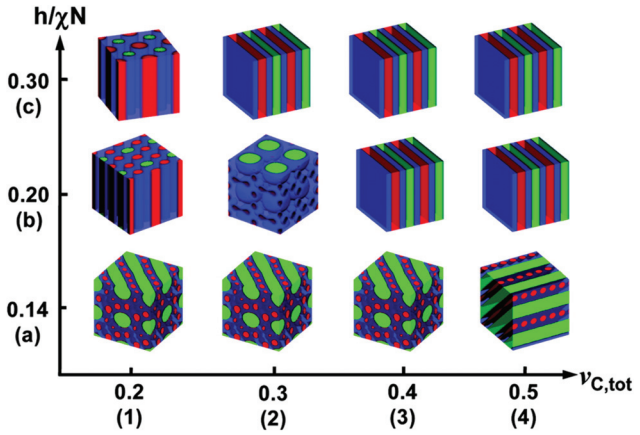

Fig. 13 Hierarchical nanostructures as a function of the total C volume fraction for the supramolecular AB diblock copolymer/C homopolymer blends at different bond strengths (a) $h/\chi N$ = 0.14, (b) $h/\chi N$ = 0.20, and (c) $h/\chi N$ = 0.30. Adapted with permission from ref. 194. Copyright 2011, American Chemical Society.

The results of simulation investigations on blends of copolymers indicate that blends of copolymers with supermolecular interactions could produce a diverse array of nanostructures, including classical and hierarchical nanostructures. With the introduction of supermolecular interactions, supermolecular multiblock, graft or star-shaped copolymers could be formed.[8,194,195,197,198] Therefore, it is possible to obtain the required structures from copolymer blends, instead of synthesizing complex copolymers *via* a complicated polymerization. In addition, the supramolecular blend systems would produce periodic nanoporous or related hybrid materials for applications in fields such as photovoltaic devices. For example, Sary *et al.* proposed a new approach to design bicontinuous electron-donor/electron-acceptor networks based on rod–coil poly(3-hexylthiophene)-poly(4-vinylpyridine) (P3HT-P4VP) block copolymers blended with [6,6]-phenyl-C_{61}-butyric acid methyl ester (PCBM) *via* supramolecular weak interactions.[199] Following this route, they successfully fabricated devices with highly improved thermal stabilities and photon-to-current conversion efficiencies. However, the understanding of the supramolecular blend is not deep enough for the preparation of advanced materials for applications. Theoretical simulations, which are performed to get to know the effects of blend ratios, supermolecular interactions and blend components on the architecture and self-assembly behaviour of supermolecular block copolymers, can help us understand how to control the structures of these blending systems and, ultimately, the device performance.

As mentioned above, theoretical simulations of self-assembly behaviours of copolymer systems have demonstrated that nanostructures can be controlled by tailoring the molecular architectures. In addition, placing copolymers into confinement and blending copolymers can also be used to control the self-assembled nanostructures. It would be time-saving and economical if we know how to design molecular architectures

Table 1 Self-assembled nanostructures and the corresponding copolymers

Nanostructures	Copolymers	Ref.
Lamellae	Most copolymer systems	
Cylinders	Most copolymer systems	
Spheres	Most copolymer systems	
Gyroid	Most copolymer systems	
Smectic A and smectic C phases	Rod–coil diblock copolymers	55, 57
	Rod–coil multiblock copolymers	107
Wavy lamellar phase	Rod–coil diblock copolymers	55
Zig-zag phase	Rod–coil diblock copolymers	54, 55, 57
Columnar square packed structure	Dendritic copolymers	183
Columnar rectangular packed structure	Dendritic copolymers	183
Chiral undulated lamellar phase	Chiral diblock copolymers	69
hexagonally ordered helices	Chiral diblock copolymers	69–71
Core–shell structures	ABC triblock copolymers	92, 98
	$A_{m+1}(BC)_m$ graft copolymers	152
Janus particles	Copolymers under spherical confinement	121
Patchy nanoparticles	Copolymers under spherical confinement	121
Knitting pattern	ABC triblock copolymers	91, 100
Tilting patterns	ABC star copolymers	166–168, 174
	ABC dendrimers	179
A15 phase	Multiply branched block copolymers	182
Complex mesocrystals	$B_1AB_2CB_3$ multiblock terpolymers	111
Fddd phase	AB type block copolymers with various architectures	76
	ABC triblock copolymers	37, 90
Parallel lamellae-in-lamella	AB rod–coil multiblock copolymers	107
	AB coil-comb block copolymers	151
	A-*b*-(B-*g*-C) graft copolymers	154, 155
	$A(BC)_n$ multiblock copolymers	105
Perpendicular lamellae-in-lamella	AB coil-comb block copolymers	151
	$A(BC)_n$ multiblock copolymers	105
	A-*b*-(B-*g*-C) graft copolymers	154, 155
Parallel cylinders-in-lamella	AB coil-comb block copolymers	151
	ABC star copolymers	166, 167, 174
Lamellae-in-cylinder	$A(BC)_n$ multiblock copolymers	105
Cylinders-in-cylinder	AB coil-comb block copolymers	151
	$A(BC)_n$ multiblock copolymers	105
	Blends of copolymers	194
Super cylinders including cylinders-on-cylinder	ABC triblock copolymers	101
and helices-on-cylinder	Block copolymers confined in pores	114, 119, 175, 176
Perpendicular cylinders-in-lamella	ABC star copolymers	166, 174
	A-*b*-(B-*g*-C) graft copolymers	154, 155
Lamellar phase with beads inside	$A_{m+1}(BC)_m$ graft copolymers	152
	ABC star copolymers	167
Lamellae-in-sphere	$A(BC)_n$ multiblock copolymers	105
	ABC star copolymers	167
Spheres around cylinder	Blends of copolymers	194
Spheres around sphere	Blends of copolymers	194

for desired materials. Therefore, we summarize the nanostructures predicted by theoretical simulations and the corresponding copolymer systems, as shown in Table 1. However, because new copolymers and nanostructures always appear, it is impossible to contain all the nanostructures and the corresponding copolymers in this table.

6. Functional properties of nanostructures self-assembled from copolymer systems

Copolymers offer the possibility of substantial improvements in materials properties, such as photovoltaic, optical and mechanical properties. To design materials based on copolymer systems with the expected functional properties, we need to not only predict the polymer structure, but also know the relation between the structures and properties. Determining the structure–property relationship to facilitate the design of materials with improved properties is one of the important tasks for copolymer systems research. Theoretical simulations offer a useful approach to get to know the structure–property relationships of copolymer systems. The significant advances in this area in recent years are featured in this section.

6.1 Photovoltaic properties

The design and fabrication of a high-efficiency polymer-based photovoltaic device requires precise control over the nanoscale morphology, molecular ordering, and interfacial properties of all components comprising the device.[200–204] With various ordered nanostructures, copolymers offer a rational and prag-

matic route for the preparation of highly efficient photovoltaic devices. However, their usefulness in these applications is currently limited due to the low level of optimization of their performance and durability. For performance improvement, many theoretical studies have been conducted to understand the relationship between the nanostructures and photovoltaic properties. There are two kinds of computational models for theoretical simulations that can be used to correlate the photovoltaic properties with the morphology: continuum and discrete models. The continuum model based on drift-diffusion equations is known as the drift-diffusion model.[205] The drift-diffusion model involves the electric potential and the charge carrier number densities of electrons, holes and excitons. Different from the continuum model, the discrete model is based on the carriers' hopping transporting mechanism in organic materials.[206,207] In the discrete model, the dynamic Monte Carlo algorithm is used to deal with the carriers' hopping process.

Theoretical simulations are a useful method to understand correlations between photovoltaic properties and ordered nanostructures of copolymer self-assemblies. Buxton *et al.* developed a drift-diffusion model capturing the transient behaviour of electrons, holes and exciton concentrations in heterogeneous polymer solar cells.[205,208] The model used the outputs from the morphological studies as the input for simulations of the photovoltaic property to elucidate the effect of the nanostructures in the system on its photovoltaic properties. Their simulation results showed that surface-induced ordering and electric-field-induced alignment can be combined to create ideal morphologies for a high photovoltaic performance. Shah *et al.* extended Buxton's model to study the effect of the morphologies on the photovoltaic properties of rod–coil block copolymers.[209] They calculated the morphology of confined rod–coil diblock copolymers using SCFT and obtained perpendicular lamellae (Fig. 14a shows the schematic of perpendicular multilayer morphology). It was noted that the rods are aligned parallel to the confining surfaces in the perpendicular lamellae. Because the influence of the molecular orientation on device performance has been shown experimentally, they rendered the mobility of holes and excitons to be an anisotropic tensor to study the effect of the rod block orientation on the performance. They examined the effect of domain spacing (D, which is directly proportional to the value of the segment size asymmetry ratio β) for rod–coil block copolymers on the short-circuit current ($|J_{sc}|$) in the case of isotropic and anisotropic charge transport, respectively. As the anisotropic strength of charge transport changes from 0 (isotropic) to 0.67 (anisotropic), the optimized domain size shifts from 2 nm to 5 nm, as shown in Fig. 14b. They demonstrated that the perpendicularly oriented lamellar morphology with an optimal domain spacing and optimal degree of anisotropy led to the highest efficiencies.

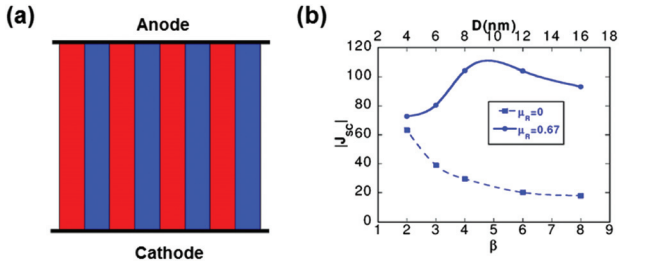

Fig. 14 (a) Schematic of the perpendicular multilayer morphology. (b) Plots of the short-circuit current $|J_{sc}|$ as a function of domain spacing D (proportional to β) for rod–coil block copolymers. Adapted with permission from ref. 209. Copyright 2010 American Chemical Society.

Because the drift-diffusion model is unable to fully consider the effect of three-dimensional structures, the dynamic Monte Carlo approach has also been used to study the effect of nanostructures on the performance of polymer solar cells. For example, Kimber *et al.* compared the photovoltaic performance of bicontinuous structures with the cylinder structure using a dynamic Monte Carlo algorithm.[210] The bicontinuous and cylinder structures, and the corresponding photovoltaic properties, including the IQE (internal quantum efficiency), FF (fill factor) and PCE (power conversion efficiency), are shown in Fig. 15. As can be seen in Fig. 15(d)–(f), the morphology type had only a slight effect on the optimum feature size, which was close to the exciton diffusion length in each case. They concluded that bicontinuous, triply periodic minimal surface morphologies might not enhance the efficiency of polymer blend solar cells. Vertical cylinder structures, if can be fabricated defect free, may be the best option because they exhibit a far superior performance than the other tested structures.

More recently, Donets *et al.* studied the photovoltaic properties of nanostructured AD diblock- and ADA triblock-copolymer systems.[211] They applied the self-consistent field theory method to generate the equilibrium nanostructured morphologies. Then, a dynamic Monte Carlo algorithm was used to model the elementary photovoltaic processes. For the morphology, they observed that both block-copolymer systems form nanostructures with a large number of bottlenecks and dead ends in the regime of high χ-parameters. This leads to a large number of charge losses in the nanostructures formed from both block-copolymer systems in the regime of high χ-parameters. As a result, there is a significant drop in the charge transport efficiency (CTE) and IQE for both types of block-copolymer systems in this parameter range. By comparing the IQE curves of both polymer systems, they deduced that the diblock-copolymer system possesses a slightly higher IQE than the triblock-copolymer system.

Theoretical simulation studies have improved the understanding of the relationship between the nanostructures and photovoltaic properties. However, the performance of all-polymer solar cells based on block copolymers has not been perfected, as expected, partially because of the long-range disordered and uncontrolled nanostructures of the block copolymers confined in these all-polymer solar cells.[212] Because of the significant influence of the molecular orientation (molecular level), domain orientation, domain size and micro-

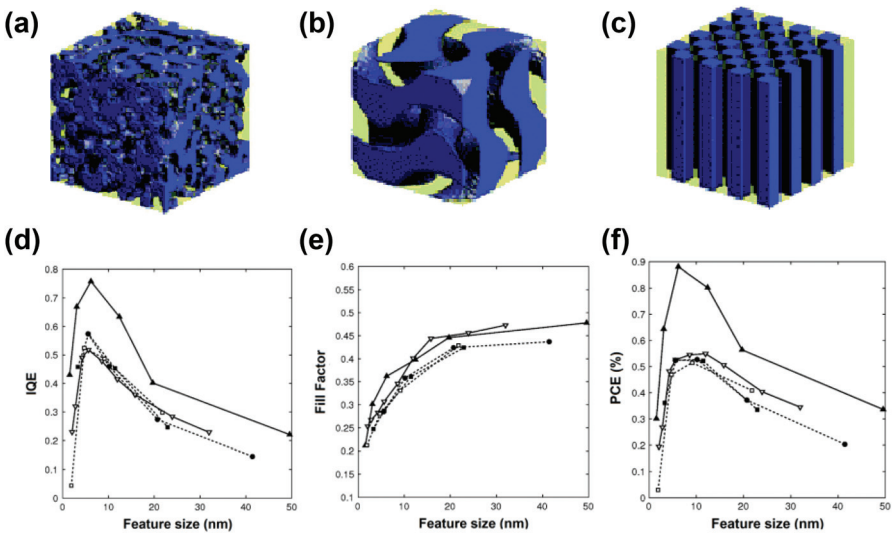

Fig. 15 (a)–(c) Examples of ordered structures investigated in ref. 210. Disordered blend (a), double gyroid (b) and cylinder (c) structures. (d)–(f) Photovoltaic properties of these five ordered structures. (d) IQE, (e) FF and (f) PCE as a function of the feature size for blends (solid line, ▽), cylinders (solid line, ▲), gyroids (dashed line, ●), double gyroid (dashed line, ■) and double diamond (dashed line, □). Reproduced with permission from ref. 210. Copyright 2010, The Royal Society of Chemistry.

domain structures (mesoscopic level) on the device performance, appropriate control of the structures from the molecular level to the mesoscopic level could promise a higher photovoltaic performance. Controlling the structures can be achieved by techniques such as directed self-assembly by a chemical patterned surface or external fields.[213,214] However, obtaining devices with an optimized morphology and molecular orientation in experiments requires a large number of trials and tests. Fortunately, theoretical simulations can be used to design the optimized devices with appropriately controlled structures, which is one of the topics we are interested in.

6.2 Optical properties

The internal microstructure of a material can be just as important as the chemistry in determining its optical properties. With the remarkable richness of tunable nanostructures, the self-assembly of copolymer systems is considered as a promising pathway for tuning the optical properties of optical devices. In this subsection, we feature examples of the simulation investigations on the relationship of optical properties and self-assembled nanostructures of copolymer systems, including lamellar (1D), cylinder (2D) and network (3D) structures. The finite difference time domain technique (FDTD) is frequently applied to calculate the optical properties.[215,216] The FDTD methodology involves the discretization of Maxwell's curl equations of electromagnetism in three dimensions. Centred finite difference operators are applied on staggered grids in space and time for electric and magnetic vector field components. In particular, the simulation region is divided into Yee cells, where the electric fields are obtained at the edges of the Yee cell and the magnetic fields are obtained at the faces of the Yee cell. The FDTD method is used to calculate the electric and magnetic fields in each cell by integrating the discretized equations through a time stepping methodology where the magnetic fields are calculated half a time step later than the electric fields. The updated electromagnetic field components are only dependent on the values at previous time steps.

As the simplest ordered structures, the optical properties of the lamellae have been studied extensively. For example, Buxton *et al.* simulated the optical properties of symmetric diblock copolymers filled with nanoparticles using SCFT/DFT and FDTD techniques.[216] The morphologies obtained by SCFT/DFT and FDTD were used as input data for FDTD to examine the optical properties of the composite. In the FDTD simulation, a differentiated Gaussian pulse, encompassing a range of frequencies, was propagated toward the self-assembled structure of nanoparticle-filled diblock copolymers. The simulations revealed that changes in the chemical nature of the nanoparticles result in different spatial distributions of the particles, hence resulting in significantly different optical properties. The addition of nanoparticles increases the dielectric contrast within the system, resulting in more defined band gaps, with 100% reflectance and a wider frequency gap. In addition, the increase in the optical distance can result in a decrease in the principle frequencies of reflectance. More recently, Sun *et al.* investigated the photonic band gap properties of cylinder microdomain nanoporous films using the finite difference time-domain method.[217] These films were proposed to be treated as a type of 2-dimensional block copolymer-based photonic crystal. They calculated the gap map for the H-polarization of the nanoporous film-based photonic band gap materials as the ratio of the centre-to-centre cylinder distance to cylinder column radius (r/a) was varied. The location of the band gap increased, and the band-gap widths broadened as the r/a ratio increased. In addition to the 1D and

2D structures, the 3D-network structured materials also possess a host of interesting optical properties.[218–220] To study the optical properties of ordered network structures, Maldovan *et al.* calculated the band structures of three dimensionally periodic bi- and tricontinuous cubic structures using the plane-wave method to solve Maxwell's equations.[221] They predicted that the morphologies of the 3D continuous block copolymer network could exhibit complete photonic band gaps.

The outstanding optical property of the 3D continuous network nanostructures has been confirmed by Vignolini and coworkers using combination studies of theoretical simulations and experiments.[222–224] Vignolini *et al.* fabricated a 3D gyroid network based on the self-assembled structures of block copolymers, as shown in Fig. 16(a).[222] In the simulations, they utilized SCFT to simulate the gyroid morphology formed by a realistic triblock copolymer. The transmittance, reflectance, and absorption of the gyroid film were simulated using an FDTD simulator. The FDTD calculations successfully reproduce the experimental measurements, as shown in Fig. 16(b). The transmission of circularly polarized light is maximal for the two rotation angles (0° and 180°). Along one of the chiral axes, either left or right circularly polarized light was preferentially transmitted, depending on the chirality of the morphology. Their results indicated that this material with the gyroid network structure is continuous with a 10 nm length scale, and it exhibits orientation-dependent colour under linearly polarized incident light as well as optical chirality. These findings can provide guidelines to facilitate the design of photonic band gap materials.

As mentioned above, ordered structures self-assembled from copolymers with the addition of nanoparticles exhibit high optical properties. Therefore, it can be predicted that films of block copolymer-tethered nanoparticles could also possess high optical properties. Lin *et al.* predicted the hierarchical structures of these systems of block copolymer-tethered nanoparticles.[225] However, there are few studies on the optical properties of the hierarchical structures. Before these hierarchical structures can be used as optical materials, their optical properties should be well understood, which could be investigated using theoretical simulations.

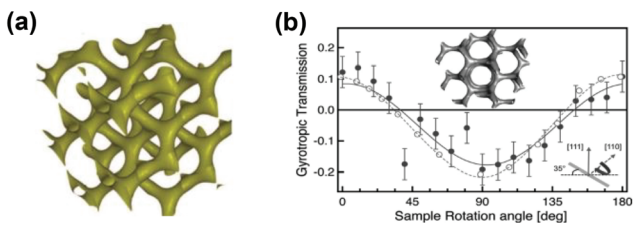

Fig. 16 (a) 3D continuous gold network. (b) Gyrotropic transmission through a sample inclined at 35°. The open symbols are the result of a finite difference time domain calculation, while the filled-in symbols are the measurements. The lines provide a visual guide. Adapted with permission from ref. 222. Copyright 2012, Wiley-VCH.

6.3 Mechanical properties

The self-assembly of copolymers provides a method for creating materials with improved mechanical properties. One of the challenges in designing these materials with improved mechanical properties is to predict the macroscopic behaviours of the self-assembled structures of copolymer systems. Theoretical simulations have been performed to understand and predict the relationship between the nanostructures and the mechanical properties. Below we present recent studies on the mechanical properties of copolymer systems investigated by theoretical simulations.

Soto-Figueroa *et al.* correlated the mechanical properties to the morphology of PS-*b*-PI and PS-*b*-PMMA diblock copolymers using molecular modelling and numerical simulations.[226] They obtained the morphologies of lamellar, body-centred cubic, hexagonal-packed cylinder, and gyroid nanostructures as the PS fraction varied in the coarse-grained molecular dynamics simulations. The mechanical properties of these block copolymers were predicted by semi-empirical and empirical relationships developed by Seitz.[227] It was found that the mechanical properties of both diblock copolymers were dependent on the PS fraction, while the variance of the PS fraction led the nanostructure transition. These simulation results indicate that the mechanical properties exhibited by the block copolymers are affected by the morphology.

Recently, Deng *et al.* adopted a combined simulation method that utilized the MesoDyn method, which is based on dynamic mean-field density functional theory, for morphologies and the probabilistic lattice spring model to study the mechanical properties of block copolymers.[228] They found that stiffness is controlled by the hard phase network, which is largely invariant to the shrinkage of the phase domain. To investigate the effect of morphology on the mechanical properties, they constructed a one-dimensional lamella to serve as a basic unit in the microstructure and studied the orientation effect of the lamella on the mechanical properties. Both the Young's modulus and fracture strain were found to be dependent on the tensile stress direction, indicating that the mechanical properties are sensitive to the morphology.

The molecular architecture is also known to influence the mechanical properties of copolymers. This effect has been investigated using simulations. For example, Zhang *et al.* studied the influence of graft number and junction points on the elasticity of graft copolymer melts using real space SCFT.[6] Graft copolymers with a larger branch number were found to exhibit better mechanical properties. To understand the effect of junction distribution on the moduli, they divided the internal energy into the energy from respective blocks of the backbone. It was found that the moduli contributed from the internal energy of different blocks of the backbone are associated with their lengths.

Despite the classically ordered nanostructures, complex nanostructures, such as hierarchical structures, have shown excellent mechanical properties in many studies.[229–231] To understand how the hierarchical structures determine the

mechanical properties of materials, Lin *et al.* elucidated the mechanical properties of $A(BC)_n$ multiblock copolymers with hierarchical lamellae-in-lamella structures, using real space SCFT.[232] Fig. 17(a)–(c) show several representative density profiles at different stages of separation. The top images in the figures show the corresponding two-dimensional structures. As shown, a weakly segregated lamellar structure is observed when the interaction strength $\chi N = 48$, and a strongly separated lamellae-in-lamellar structure emerges at higher values of interaction strength. The mechanical properties were found to increase with increasing interaction strength, as shown in Fig. 17(d)–(f). In addition, the AB block copolymer showed weaker elastic properties compared to the $A(BC)_n$ copolymers when $\chi N > 48$. According to their simulation results, it can be concluded that the $A(BC)_n$ multiblock copolymers with a lamellae-in-lamella structure have apparent advantages over the simple diblock copolymers regarding the mechanical properties. The enhanced mechanical properties are primarily attributed to the interplay of the internal energy and conformational entropy of BC blocks.

Theoretical simulation studies of the structure–property relationship have shown that the macroscopic properties of a copolymer system can be significantly improved by carefully tailoring the self-assembling nanostructures. However, because of the remarkable richness of nanostructures self-assembled from copolymer systems, the understanding of the structure–property relationship is not deep enough to facilitate the fabrication of high performance structures. An open question remains about how excellent properties can be achieved by preparing the materials with ordered nanostructures. This problem has gained new impetus from the combination of theoretical simulations and experimental efforts.

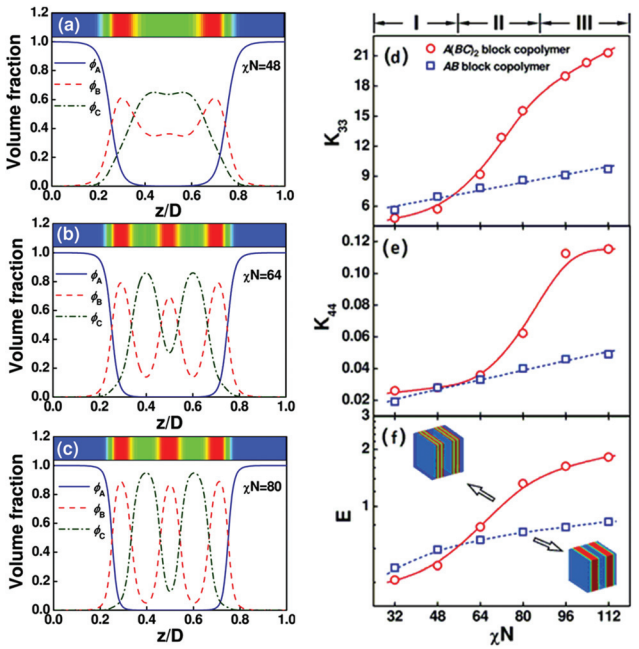

Fig. 17 One-dimensional density profiles of A, B, and C blocks of $A(BC)_2$ multiblock copolymers with $f_A = 0.5$ along the *z*-direction at various χN: (a) $\chi N = 48$, (b) $\chi N = 64$, and (c) $\chi N = 80$. The top images show the corresponding two-dimensional structures. (d), (e) and (f) Show the dimensionless extensional, shear and Young's moduli (K_{33}, K_{44}, E) as a function of χN for $A(BC)_2$ multiblock copolymers and AB diblock copolymers, respectively. The interaction strength in diblock copolymers is the same as χN. Adapted with permission from ref. 232. Copyright 2011, American Chemical Society.

7. Conclusions and outlook

Nanostructures self-assembled from copolymers have attracted considerable attention in recent years. In this review, an overview of the simulation investigations about the self-assembled nanostructures and the structure–property relationship in copolymer systems is presented. Many studies have demonstrated that nanostructures can be controlled by tailoring the molecular architectures. In addition, placing copolymers into confinement can also be used to control the self-assembly, leading to the development of methods to engineer novel nanostructures that are not available from bulk copolymers. Moreover, the formation kinetics of the self-assembled nanostructures and their dependence on the molecular parameters of copolymers are also summarized. Tailoring the kinetic factors has been presented as another approach to control the self-assembled structures. The self-assembled nanostructures, which can be controlled *via* the paths discussed, have been demonstrated to play an important role in determining the functional properties, such as photovoltaic, optical and mechanical properties. Theoretical simulations could ultimately reveal the effects of the choices in the initial design state of the materials on the final performance, facilitating the efficient fabrication of copolymer systems with the desired functional properties.

While many advances have been reported in the studies of nanostructures self-assembled from copolymer systems, there are still many challenges and opportunities for designing nanostructures self-assembled from copolymer systems with the desired functional properties.

(a) Obtaining functional properties: with the advancement in copolymer synthesis, copolymers consisting of blocks with functional properties can be obtained. These functional copolymers can self-assemble into ordered nanostructures. This functional self-assembly provides a unique approach to achieve new properties. Furthermore, multiblock copolymers consisting of blocks with different functional properties can self-assemble into ordered multifunctional structures. The microscopic functionalities of these copolymer systems can be transferred or amplified to the macroscopic level *via* self-assembly. These functional nanostructures can be widely used in the fields of microelectronic devices, micro-reactors, biochemical sensors and optical devices. However, questions remain as to whether and how the molecular functions are transferred or amplified through nanostructures to macroscopic properties.

(b) Combining studies of theoretical simulations and experiments: to better understand and exert control over the self-assembled structure of copolymer systems, a close collaboration between experimental studies and theoretical predictions is required. On the one hand, it is time consuming to investigate the self-assembly of copolymers by experimental trials and tests. On the other hand, the validity of simulation results should be confirmed by comparing them with experimental observations. In the future, the combination of simulations and experiments will be a promising method to precisely fabricate nanostructures formed from copolymer systems. To achieve this goal, the techniques that map the molecular parameters in the simulation model and the realistic experiments should be further developed.

(c) Precisely predicting the functional properties: most of the theoretical simulations on copolymer systems focused on morphology studies. In contrast, the functional properties, such as photovoltaic, electrical and magnetic properties, exhibited by the copolymer systems have not been widely studied. Before these copolymers can be used as functional materials, the structure–property relationships should be well understood, which could be investigated using theoretical simulations. The functional properties of copolymer systems are significantly affected by the phenomena arising on different length and time scales. Theoretical simulations aiming to precisely predict material hierarchical structures and properties are required to cover a wider range of length and time scales. As one of these simulation techniques, multiscale modelling is under development to precisely predict the structures and properties of copolymer systems. However, the notion of selecting or disregarding subscale information requires interdisciplinary methods, such as self-consistent methods and percolation theory, to average out the effect within the continuum.

(d) Designing copolymers and processing for desired functional materials: it can be envisioned that the development of materials would begin with the function and can be aided by theoretical simulations in the selection of the appropriate building blocks and processes. Designing copolymers and processing for desired functional materials is a reverse problem, which can avoid most of the experimental trials and tests. Because of the diversity of copolymers and the large number of corresponding nanostructures, the solution of the reverse problem for copolymer systems will be beneficial in fabricating functional materials formed from copolymers. Obtaining the solutions of the reverse problem requires genetic algorithms or other techniques for global optimization or requires theoretical simulation tools that will be developed in the future.

Abbreviations

CGMD	Coarse-grained molecular dynamics
BD	Brownian dynamics
DPD	Dissipative particle dynamics
MC	Monte Carlo simulations
TDGL	Time-dependent Ginzburg–Landau
DDFT	Dynamic density functional theory
SCFT	Self-consistent field theory
L	Lamellar phase
G	Gyroid phase
C	Cylinder phase
S	Sphere phase
PS-*b*-PI	Polystyrene-*b*-polyisoprene
OOT	Order–order transition
ODT	Order–disorder transition
ISO	Poly(isoprene-*b*-styrene-*b*-ethylene oxide)
SEBM	Polystyrene-*b*-poly(ethylene-*co*-butylene)-*b*-poly(methyl methacrylate)
PS-*g*-PI	Polystyrene-*g*-polyisoprene
PFP-*g*-P2VP	Poly(fluorene-*alt*-phenylene)-*g*-poly(2-vinylpyridine)
SCLC	Side chain liquid crystalline
LC	Liquid crystalline
VCS	Variable cell shape
IQE	Internal quantum efficiency
FF	Fill factor
PCE	Power conversion efficiency
J_{sc}	Short-current density
P3HT-P4VP	Poly(3-hexylthiophene)-poly(4-vinylpyridine)
PCBM	[6,6]-Phenyl-C_{61}-butyric acid methyl ester
PS-*b*-PMMA	Polystyrene-*b*-poly(methyl methacrylate)
FDTD	Finite difference time domain

Acknowledgements

This work was supported by the National Natural Science Foundation of China (21234002, 21474029, 51303055 and 51573049) and the National Basic Research Program of China (2012CB933600). Support from Projects of Shanghai municipality (13JC1402000) is also appreciated.

References

1 F. S. Bates and G. H. Fredrickson, *Annu. Rev. Phys. Chem.*, 1990, **41**, 525–557.
2 T. E. Kang, K.-H. Kim and B. J. Kim, *J. Mater. Chem. A*, 2014, **2**, 15252–15267.
3 J. Fang, Z. Wang, J. Zhang, Y. Zhang, D. Deng, Z. Wang, K. Lu, W. Ma and Z. Wei, *Adv. Sci.*, 2015, **2**, 1500250.
4 W. Lee, J.-S. Kim, H. J. Kim, J. M. Shin, K. H. Ku, H. Yang, J. Lee, J. G. Bae, W. B. Lee and B. J. Kim, *Macromolecules*, 2015, **48**, 5563–5569.
5 G. Hauffman, A. Vlad, T. Janoschka, U. S. Schubert and J. F. Gohy, *J. Mater. Chem. A*, 2015, **3**, 19575–19581.
6 L. Zhang, J. Lin and S. Lin, *Soft Matter*, 2009, **5**, 173–181.
7 Y. Mai and A. Eisenberg, *Chem. Soc. Rev.*, 2012, **41**, 5969–5985.

8 L. Wang, J. Lin and X. Zhang, *Polymer*, 2013, **54**, 3427–3442.
9 T. P. Lodge, *Macromol. Chem. Phys.*, 2003, **204**, 265–273.
10 F. S. Bates, M. A. Hillmyer, T. P. Lodge, C. M. Bates, K. T. Delaney and G. H. Fredrickson, *Science*, 2012, **336**, 434–440.
11 G. H. Fredrickson, V. Ganesan and F. Drolet, *Macromolecules*, 2002, **35**, 16–39.
12 F. Müller-Plathe, *ChemPhysChem*, 2002, **3**, 754–769.
13 G. S. Grest and K. Kremer, *Phys. Rev. A*, 1986, **33**, 3628–3631.
14 K. Kremer and G. S. Grest, *J. Chem. Phys.*, 1990, **92**, 5057–5086.
15 M. Kröger, *Phys. Rep.*, 2004, **390**, 453–551.
16 J. D. Weeks, D. Chandler and H. C. Andersen, *J. Chem. Phys.*, 1971, **54**, 5237–5247.
17 V. Rühle, C. Junghans, A. Lukyanov, K. Kremer and D. Andrienko, *J. Chem. Theor. Comput.*, 2009, **5**, 3211–3223.
18 S. C. Glotzer and W. Paul, *Annu. Rev. Mater. Res.*, 2002, **32**, 401–436.
19 P. J. Hoogerbrugge and J. M. V. A. Koelman, *Europhys. Lett.*, 1992, **19**, 155.
20 P. Espanol and P. Warren, *Europhys. Lett.*, 1995, **30**, 191.
21 R. D. Groot and P. B. Warren, *J. Chem. Phys.*, 1997, **107**, 4423.
22 R. D. Groot and T. J. Madden, *J. Chem. Phys.*, 1998, **108**, 8713–8724.
23 M. P. Allen and D. J. Tildesley, *Computer simulation of liquids*, Oxford University Press, Oxford, 1987.
24 D. Frenkel and B. Smit, *Understanding molecular simulation - from algorithms to applications*, Academic, San Diego, 2002.
25 Q. Wang, P. F. Nealey and J. J. de Pablo, *Macromolecules*, 2002, **35**, 9563–9573.
26 Y. Oono and S. Puri, *Phys. Rev. A*, 1988, **38**, 434–453.
27 J. G. E. M. Fraaije, *J. Chem. Phys.*, 1993, **99**, 9202–9212.
28 J. G. E. M. Fraaije, *J. Chem. Phys.*, 1994, **100**, 6984–6984.
29 J. G. E. M. Fraaije, B. A. C. Van Vlimmeren, N. M. Maurits, M. Postma, O. A. Evers, C. Hoffmann, P. Altevogt and G. Goldbeck-Wood, *J. Chem. Phys.*, 1997, **106**, 4260–4269.
30 G. H. Fredrickson, *The Equilibrium Theory of Inhomogeneous Polymers*, Oxford University Press, New York, 2006.
31 S. F. Edwards, *Proc. Phys. Soc.*, 1965, **85**, 613.
32 X. Li, D. Kou, S. Rao and H. Liang, *J. Chem. Phys.*, 2006, **124**, 204909.
33 G. Milano and T. Kawakatsu, *J. Chem. Phys.*, 2010, **133**, 214102.
34 A. De Nicola, T. Kawakatsu and G. Milano, *J. Chem. Theor. Comput.*, 2014, **10**, 5651–5667.
35 H. Hu, M. Gopinadhan and C. O. Osuji, *Soft Matter*, 2014, **10**, 3867–3889.
36 M. W. Matsen and F. S. Bates, *Macromolecules*, 1996, **29**, 1091–1098.
37 C. A. Tyler and D. C. Morse, *Phys. Rev. Lett.*, 2005, **94**, 208302.
38 M. Takenaka, T. Wakada, S. Akasaka, S. Nishitsuji, K. Saijo, H. Shimizu, M. I. Kim and H. Hasegawa, *Macromolecules*, 2007, **40**, 4399–4402.
39 M. I. Kim, T. Wakada, S. Akasaka, S. Nishitsuji, K. Saijo, H. Hasegawa, K. Ito and M. Takenaka, *Macromolecules*, 2008, **41**, 7667–7670.
40 M. W. Matsen, *Phys. Rev. Lett.*, 2007, **99**, 148304.
41 D. M. Cooke and A.-C. Shi, *Macromolecules*, 2006, **39**, 6661–6671.
42 T. M. Beardsley and M. W. Matsen, *Macromolecules*, 2011, **44**, 6209–6219.
43 N. A. Lynd and M. A. Hillmyer, *Macromolecules*, 2007, **40**, 8050–8055.
44 Y. Li, H.-J. Qian and Z.-Y. Lu, *Polymer*, 2013, **54**, 3716–3722.
45 M. Lee, B.-K. Cho and W.-C. Zin, *Chem. Rev.*, 2001, **101**, 3869–3892.
46 E. L. Thomas, J. T. Chen, M. J. E. O'Rourke, C. K. Ober and G. Mao, *Macromol. Symp.*, 1997, **117**, 241–256.
47 H. Tu, X. Wan, Y. Liu, X. Chen, D. Zhang, Q.-F. Zhou, Z. Shen, J. J. Ge, S. Jin and S. Z. D. Cheng, *Macromolecules*, 2000, **33**, 6315–6320.
48 M. Lee, B.-K. Cho, H. Kim, J.-Y. Yoon and W.-C. Zin, *J. Am. Chem. Soc.*, 1998, **120**, 9168–9179.
49 M. Lee, B.-K. Cho, H. Kim and W.-C. Zin, *Angew. Chem., Int. Ed.*, 1998, **37**, 638–640.
50 B. D. Olsen and R. A. Segalman, *Macromolecules*, 2006, **39**, 7078–7083.
51 N. Sary, L. Rubatat, C. Brochon, G. Hadziioannou, J. Ruokolainen and R. Mezzenga, *Macromolecules*, 2007, **40**, 6990–6997.
52 J. T. Chen, E. L. Thomas, C. K. Ober and S. S. Hwang, *Macromolecules*, 1995, **28**, 1688–1697.
53 L.-Y. Shi, Y. Zhou, X.-H. Fan and Z. Shen, *Macromolecules*, 2013, **46**, 5308–5316.
54 J.-Z. Chen, C.-X. Zhang, Z.-Y. Sun, Y.-S. Zheng and L.-J. An, *J. Chem. Phys.*, 2006, **124**, 104907.
55 M. A. Horsch, Z. Zhang and S. C. Glotzer, *Soft Matter*, 2010, **6**, 945–954.
56 Y. A. Kriksin and P. G. Khalatur, *Macromol. Theory Simul.*, 2012, **21**, 382–399.
57 V. Pryamitsyn and V. Ganesan, *J. Chem. Phys.*, 2004, **120**, 5824–5838.
58 M. Reenders and G. Ten Brinke, *Macromolecules*, 2002, **35**, 3266–3280.
59 W. Song, P. Tang, F. Qiu, Y. Yang and A.-C. Shi, *Soft Matter*, 2011, **7**, 929–938.
60 J. Tang, Y. Jiang, X. Zhang, D. Yan and J. Z. Chen, *Macromolecules*, 2015, **48**, 9060–9070.
61 Y. Bouligand, *C. R. Chim.*, 2008, **11**, 281–296.
62 J. W. Goodby, *J. Mater. Chem.*, 1991, **1**, 307–318.
63 C. Cai, Y. Li, J. Lin, L. Wang, S. Lin, X. S. Wang and T. Jiang, *Angew. Chem., Int. Ed.*, 2013, **52**, 7732–7736.

64 C. Cai, J. Lin, X. Zhu, S. Gong, X.-S. Wang and L. Wang, *Macromolecules*, 2016, **49**, 15–22.
65 Y.-W. Chiang, R.-M. Ho, C. Burger and H. Hasegawa, *Soft Matter*, 2011, **7**, 9797–9803.
66 R.-M. Ho, Y.-W. Chiang, C.-K. Chen, H.-W. Wang, H. Hasegawa, S. Akasaka, E. L. Thomas, C. Burger and B. S. Hsiao, *J. Am. Chem. Soc.*, 2009, **131**, 18533–18542.
67 R.-M. Ho, M.-C. Li, S.-C. Lin, H.-F. Wang, Y.-D. Lee, H. Hasegawa and E. L. Thomas, *J. Am. Chem. Soc.*, 2012, **134**, 10974–10986.
68 S. Pieraccini, S. Masiero, A. Ferrarini and G. P. Spada, *Chem. Soc. Rev.*, 2011, **40**, 258–271.
69 W. Zhao, T. P. Russell and G. M. Grason, *Phys. Rev. Lett.*, 2013, **110**, 058301.
70 W. Zhao, T. P. Russell and G. M. Grason, *J. Chem. Phys.*, 2012, **137**, 104911.
71 S.-H. Wang, T. Kawakatsu, P. Chen and C. D. Lu, *J. Chem. Phys.*, 2013, **138**, 194901.
72 M. He, F. Qiu and Z. Lin, *J. Mater. Chem.*, 2011, **21**, 17039–17048.
73 S. Wang, Q. Yang, Y. Tao, Y. Guo, J. Yang, Y. Liu, L. Zhao, Z. Xie and W. Huang, *New J. Chem.*, 2016, **40**, 1825–1833.
74 M. W. Matsen, *J. Chem. Phys.*, 2000, **113**, 5539–5544.
75 M. W. Matsen and R. B. Thompson, *J. Chem. Phys.*, 1999, **111**, 7139–7146.
76 M. W. Matsen, *Macromolecules*, 2012, **45**, 2161–2165.
77 B. L. Riise, G. H. Fredrickson, R. G. Larson and D. S. Pearson, *Macromolecules*, 1995, **28**, 7653–7659.
78 C. Y. Ryu, M. S. Lee, D. A. Hajduk and T. P. Lodge, *J. Polym. Sci., Part B: Polym. Phys.*, 1997, **35**, 2811–2823.
79 H. Watanabe, *Macromolecules*, 1995, **28**, 5006–5011.
80 M. W. Hamersky, S. D. Smith, A. O. Gozen and R. J. Spontak, *Phys. Rev. Lett.*, 2005, **95**, 168306.
81 S. S. Tallury, K. P. Mineart, S. Woloszczuk, D. N. Williams, R. B. Thompson, M. A. Pasquinelli, M. Banaszak and R. J. Spontak, *J. Chem. Phys.*, 2014, **141**, 121103.
82 E. Ibarboure, E. Papon and J. Rodriguez-Hernandez, *Polymer*, 2007, **48**, 3717–3725.
83 Z. Wang, Y. Lan, K. Zhong, Y. Liang, T. Chen and L. Y. Jin, *Int. J. Mol. Sci.*, 2014, **15**, 5634–5648.
84 G. Floudas, P. Papadopoulos, H.-A. Klok, G. W. M. Vandermeulen and J. Rodriguez-Hernandez, *Macromolecules*, 2003, **36**, 3673–3683.
85 J.-Z. Chen, Z.-Y. Sun, C.-X. Zhang, L.-J. An and Z. Tong, *J. Chem. Phys.*, 2008, **128**, 074904.
86 J.-Z. Chen, C.-X. Zhang, Z.-Y. Sun, L.-J. An and Z. Tong, *J. Chem. Phys.*, 2007, **127**, 024105.
87 M. Lee, B.-K. Cho, Y.-G. Jang and W.-C. Zin, *J. Am. Chem. Soc.*, 2000, **122**, 7449–7455.
88 Z.-X. Ma, J.-H. Huang and M.-B. Luo, *Soft Matter*, 2015, **11**, 4932–4943.
89 A. AlSunaidi, W. K. Den Otter and J. H. R. Clarke, *J. Chem. Phys.*, 2009, **130**, 124910.
90 C. A. Tyler, J. Qin, F. S. Bates and D. C. Morse, *Macromolecules*, 2007, **40**, 4654–4668.
91 Z. Guo, G. Zhang, F. Qiu, H. Zhang, Y. Yang and A.-C. Shi, *Phys. Rev. Lett.*, 2008, **101**, 028301.
92 W. Zheng and Z.-G. Wang, *Macromolecules*, 1995, **28**, 7215–7223.
93 F. S. Bates, *MRS Bull.*, 2005, **30**, 525–532.
94 T. S. Bailey, C. M. Hardy, T. H. Epps and F. S. Bates, *Macromolecules*, 2002, **35**, 7007–7017.
95 T. H. Epps, E. W. Cochran, C. M. Hardy, T. S. Bailey, R. S. Waletzko and F. S. Bates, *Macromolecules*, 2004, **37**, 7085–7088.
96 T. H. Epps, E. W. Cochran, T. S. Bailey, R. S. Waletzko, C. M. Hardy and F. S. Bates, *Macromolecules*, 2004, **37**, 8325–8341.
97 H. Elbs, V. Abetz, G. Hadziioannou, C. Drummer and G. Krausch, *Macromolecules*, 2001, **34**, 7917–7919.
98 H. Ott, V. Abetz and V. Altstädt, *Macromolecules*, 2001, **34**, 2121–2128.
99 U. Breiner, U. Krappe, E. L. Thomas and R. Stadler, *Macromolecules*, 1998, **31**, 135–141.
100 M. Liu, W. Li, F. Qiu and A.-C. Shi, *Macromolecules*, 2012, **45**, 9522–9530.
101 W. Li, F. Qiu and A.-C. Shi, *Macromolecules*, 2012, **45**, 503–509.
102 H. Jinnai, T. Kaneko, K. Matsunaga, C. Abetz and V. Abetz, *Soft Matter*, 2009, **5**, 2042–2046.
103 Y. Xia, J. Chen, Z. Sun, T. Shi, L. An and Y. Jia, *Polymer*, 2010, **51**, 3315–3319.
104 C.-J. Chang, Y.-H. Lee, H.-L. Chen, C.-H. Chiang, H.-F. Hsu, C.-C. Ho, W.-F. Su and C.-A. Dai, *Soft Matter*, 2011, **7**, 10951–10960.
105 L. Wang, J. Lin and L. Zhang, *Macromolecules*, 2010, **43**, 1602–1609.
106 X. Zhang, L. Wang, L. Zhang, J. Lin and T. Jiang, *Langmuir*, 2015, **31**, 2533–2544.
107 X. Zhu, L. Wang and J. Lin, *J. Phys. Chem. B*, 2013, **117**, 5748–5756.
108 A. A. Gavrilov, Y. V. Kudryavtsev, P. G. Khalatur and A. V. Chertovich, *Chem. Phys. Lett.*, 2011, **503**, 277–282.
109 M. Liu, B. Xia, W. Li, F. Qiu and A.-C. Shi, *Macromolecules*, 2015, **48**, 3386–3394.
110 J. Masuda, A. Takano, J. Suzuki, Y. Nagata, A. Noro, K. Hayashida and Y. Matsushita, *Macromolecules*, 2007, **40**, 4023–4027.
111 N. Xie, M. Liu, H. Deng, W. Li, F. Qiu and A.-C. Shi, *J. Am. Chem. Soc.*, 2014, **136**, 2974–2977.
112 J. K. Kim, J. I. Lee and D. H. Lee, *Macromol. Res.*, 2008, **16**, 267–292.
113 C. R. Stewart-Sloan and E. L. Thomas, *Eur. Polym. J.*, 2011, **47**, 630–646.
114 A.-C. Shi and B. Li, *Soft Matter*, 2013, **9**, 1398–1413.
115 A. Knoll, A. Horvat, K. S. Lyakhova, G. Krausch, G. J. A. Sevink, A. V. Zvelindovsky and R. Magerle, *Phys. Rev. Lett.*, 2002, **89**, 035501.
116 W. Li, M. Liu, F. Qiu and A.-C. Shi, *J. Phys. Chem. B*, 2013, **117**, 5280–5288.

117 A. Nikoubashman, R. A. Register and A. Z. Panagiotopoulos, *Macromolecules*, 2013, **46**, 6651–6658.
118 T. Zhang, H. Deng, T. Yang and W. Li, *Polymer*, 2015, **65**, 168–174.
119 P. Chen, H. Liang and A.-C. Shi, *Macromolecules*, 2007, **40**, 7329–7335.
120 B. Yu, B. Li, Q. Jin, D. Ding and A.-C. Shi, *Macromolecules*, 2007, **40**, 9133–9142.
121 B. Yu, J. Deng, B. Li and A.-C. Shi, *Soft Matter*, 2014, **10**, 6831–6843.
122 J. Xu, K. Wang, J. Li, H. Zhou, X. Xie and J. Zhu, *Macromolecules*, 2015, **48**, 2628–2636.
123 D. R. Nelson, *Nano Lett.*, 2002, **2**, 1125–1129.
124 L. Zhang, L. Wang and J. Lin, *Soft Matter*, 2014, **10**, 6713–6721.
125 I. Bita, J. K. W. Yang, Y. S. Jung, C. A. Ross, E. L. Thomas and K. K. Berggren, *Science*, 2008, **321**, 939–943.
126 J. K. W. Yang, Y. S. Jung, J.-B. Chang, R. A. Mickiewicz, A. Alexander-Katz, C. A. Ross and K. K. Berggren, *Nat. Nanotechnol.*, 2010, **5**, 256–260.
127 L. Zhang, L. Wang and J. Lin, *ACS Macro Lett.*, 2014, **3**, 712–716.
128 P. M. Chaikin and T. C. Lubensky, *Principles of condensed matter physics*, Cambridge University Press, Cambridge, 1995.
129 S. Qi and Z.-G. Wang, *Phys. Rev. Lett.*, 1996, **76**, 1679.
130 H.-W. Park, J. Jung, T. Chang, K. Matsunaga and H. Jinnai, *J. Am. Chem. Soc.*, 2009, **131**, 46–47.
131 M. W. Matsen, *J. Chem. Phys.*, 2001, **114**, 8165–8173.
132 R. A. Wickham, A.-C. Shi and Z.-G. Wang, *J. Chem. Phys.*, 2003, **118**, 10293–10305.
133 X. Cheng, L. Lin, E. Weinan, P. Zhang and A.-C. Shi, *Phys. Rev. Lett.*, 2010, **104**, 148301.
134 I. W. Hamley, V. Castelletto, O. O. Mykhaylyk, Z. Yang, R. P. May, K. S. Lyakhova, G. J. A. Sevink and A. V. Zvelindovsky, *Langmuir*, 2004, **20**, 10785–10790.
135 M. Imai, A. Saeki, T. Teramoto, A. Kawaguchi, K. Nakaya, T. Kato and K. Ito, *J. Chem. Phys.*, 2001, **115**, 10525–10531.
136 K. Yamauchi, H. Hasegawa, T. Hashimoto, N. Köhler and K. Knoll, *Polymer*, 2002, **43**, 3563–3570.
137 K. Yamauchi, H. Hasegawa, T. Hashimoto and M. Nagao, *J. Appl. Crystallogr.*, 2003, **36**, 708–712.
138 P. Maniadis, R. B. Thompson, K. Ø. Rasmussen and T. Lookman, *Phys. Rev. E: Stat. Phys., Plasmas, Fluids, Relat. Interdiscip. Top.*, 2004, **69**, 031801.
139 J. Xia, M. Sun, F. Qiu, H. Zhang and Y. Yang, *Macromolecules*, 2005, **38**, 9324–9332.
140 D. Gersappe, D. Irvine, A. C. Balazs, Y. Liu, J. Sokolov, M. Rafailovich, S. Schwarz and D. G. Peiffer, *Science*, 1994, **265**, 1072–1074.
141 R. Weidisch, S. P. Gido, D. Uhrig, H. Iatrou, J. Mays and N. Hadjichristidis, *Macromolecules*, 2001, **34**, 6333–6337.
142 L. Wang, L. Zhang and J. Lin, *J. Chem. Phys.*, 2008, **129**, 114905.
143 L. Zhang, J. Lin and S. Lin, *J. Phys. Chem. B*, 2008, **112**, 9720–9728.
144 C. Lee, S. P. Gido, Y. Poulos, N. Hadjichristidis, N. B. Tan, S. F. Trevino and J. W. Mays, *Polymer*, 1998, **39**, 4631–4638.
145 M. Xenidou, F. L. Beyer, N. Hadjichristidis, S. P. Gido and N. B. Tan, *Macromolecules*, 1998, **31**, 7659–7667.
146 Y. Zhu, E. Burgaz, S. P. Gido, U. Staudinger, R. Weidisch, D. Uhrig and J. W. Mays, *Macromolecules*, 2006, **39**, 4428–4436.
147 Y. Zhu, R. Weidisch, S. P. Gido, G. Velis and N. Hadjichristidis, *Macromolecules*, 2002, **35**, 5903–5909.
148 L. Zhang, J. Lin and S. Lin, *J. Phys. Chem. B*, 2007, **111**, 351–357.
149 R. J. Nap, C. Kok, G. ten Brinke and S. I. Kuchanov, *Eur. Phys. J. E*, 2001, **4**, 515–519.
150 R. J. Nap and G. ten Brinke, *Macromolecules*, 2002, **35**, 952–959.
151 L. Wang, J. Lin and L. Zhang, *Langmuir*, 2009, **25**, 4735–4742.
152 Z. Jiang, R. Wang and G. Xue, *J. Phys. Chem. B*, 2009, **113**, 7462–7467.
153 Z. Qian and R. Wang, *Macromolecules*, 2011, **44**, 6113–6120.
154 C.-I. Huang, *React. Funct. Polym.*, 2009, **69**, 530–538.
155 C. I. Huang and Y. C. Lin, *Macromol. Rapid Commun.*, 2007, **28**, 1634–1639.
156 S. Lin, Y. Wang, C. Cai, Y. Xing, J. Lin, T. Chen and X. He, *Nanotechnology*, 2013, **24**, 085602.
157 A. Martínez-Felipe, C. T. Imrie and A. Ribes-Greus, *Ind. Eng. Chem. Res.*, 2013, **52**, 8714–8721.
158 A. J. Soininen, I. Tanionou, N. ten Brummelhuis, H. Schlaad, N. Hadjichristidis, O. Ikkala, J. Raula, R. Mezzenga and J. Ruokolainen, *Macromolecules*, 2012, **45**, 7091–7097.
159 Y. Wang, S. Lin, M. Zang, Y. Xing, X. He, J. Lin and T. Chen, *Soft Matter*, 2012, **8**, 3131–3138.
160 X. Li, F. Huang, T. Jiang, X. He, S. Lin and J. Lin, *RSC Adv.*, 2015, **5**, 1514–1521.
161 M. Yamada, T. Iguchi, A. Hirao, S. Nakahama and J. Watanabe, *Polym. J.*, 1998, **30**, 23–30.
162 R. Verduzco, X. Li, S. L. Pesek and G. E. Stein, *Chem. Soc. Rev.*, 2015, **44**, 2405–2420.
163 B. R. Sveinbjörnsson, R. A. Weitekamp, G. M. Miyake, Y. Xia, H. A. Atwater and R. H. Grubbs, *Proc. Natl. Acad. Sci. U. S. A.*, 2012, **109**, 14332–14336.
164 A. Chremos and P. E. Theodorakis, *ACS Macro Lett.*, 2014, **3**, 1096–1100.
165 S. J. Dalsin, T. G. Rions-Maehren, M. D. Beam, F. S. Bates, M. A. Hillmyer and M. W. Matsen, *ACS Nano*, 2015, **9**, 12233–12245.
166 W. Xu, K. Jiang, P. Zhang and A.-C. Shi, *J. Phys. Chem. B*, 2013, **117**, 5296–5305.
167 T. Gemma, A. Hatano and T. Dotera, *Macromolecules*, 2002, **35**, 3225–3237.
168 G. Zhang, F. Qiu, H. Zhang, Y. Yang and A.-C. Shi, *Macromolecules*, 2010, **43**, 2981–2989.

169 K. Hayashida, N. Saito, S. Arai, A. Takano, N. Tanaka and Y. Matsushita, *Macromolecules*, 2007, **40**, 3695–3699.
170 A. Takano, W. Kawashima, A. Noro, Y. Isono, N. Tanaka, T. Dotera and Y. Matsushita, *J. Polym. Sci., Part B: Polym. Phys.*, 2005, **43**, 2427–2432.
171 Y. Matsushita, K. Hayashida, T. Dotera and A. Takano, *J. Phys.: Condens. Matter*, 2011, **23**, 284111.
172 Y. Matsushita, A. Takano, K. Hayashida, T. Asari and A. Noro, *Polymer*, 2009, **50**, 2191–2203.
173 A. Takano, S. Wada, S. Sato, T. Araki, K. Hirahara, T. Kazama, S. Kawahara, Y. Isono, A. Ohno, N. Tanaka and Y. Matsushita, *Macromolecules*, 2004, **37**, 9941–9946.
174 K. Jiang, J. Zhang and Q. Liang, *J. Phys. Chem. B*, 2015, **119**, 14551–14562.
175 W. Han, P. Tang, X. Li, F. Qiu, H. Zhang and Y. Yang, *J. Phys. Chem. B*, 2008, **112**, 13738–13748.
176 M. Liu, W. Li and F. Qiu, *J. Chem. Phys.*, 2013, **138**, 104904.
177 S. Li, Y. Jiang and J. Z. Chen, *Soft Matter*, 2013, **9**, 4843–4854.
178 X. Cao, L. Zhang, L. Wang and J. Lin, *Soft Matter*, 2014, **10**, 5916–5927.
179 B. Lin, H. Zhang, P. Tang, F. Qiu and Y. Yang, *Soft Matter*, 2011, **7**, 10076–10084.
180 G. M. Grason, B. A. DiDonna and R. D. Kamien, *Phys. Rev. Lett.*, 2003, **91**, 058304.
181 F. Wurm and H. Frey, *Prog. Polym. Sci.*, 2011, **36**, 1–52.
182 G. M. Grason and R. D. Kamien, *Phys. Rev. E: Stat. Phys., Plasmas, Fluids, Relat. Interdiscip. Top.*, 2005, **71**, 051801.
183 W. B. Lee, R. Elliott, R. Mezzenga and G. H. Fredrickson, *Macromolecules*, 2009, **42**, 849–859.
184 B. Wenn, A. C. Martens, Y. M. Chuang, J. Gruber and T. Junkers, *Polym. Chem.*, 2016, **7**, 2720–2727.
185 C. Lee, S. P. Gido, Y. Poulos, N. Hadjichristidis, N. B. Tan, S. F. Trevino and J. W. Mays, *J. Chem. Phys.*, 1997, **107**, 6460–6469.
186 X. Ye, T. Shi, Z. Lu, C. Zhang, Z. Sun and L. An, *Macromolecules*, 2005, **38**, 8853–8857.
187 X. Ye, X. Yu, Z. Sun and L. An, *J. Phys. Chem. B*, 2006, **110**, 12042–12046.
188 J. Peng, X. Gao, Y. Wei, H. Wang, B. Li and Y. Han, *J. Chem. Phys.*, 2005, **122**, 114706.
189 D. Q. Pike, M. Müller and J. J. de Pablo, *J. Chem. Phys.*, 2011, **135**, 114904.
190 J. Yang, Q. Wang, W. Yao, F. Chen and Q. Fu, *Appl. Surf. Sci.*, 2011, **257**, 4928–4934.
191 K. Dobrosielska, A. Takano and Y. Matsushita, *Macromolecules*, 2010, **43**, 1101–1107.
192 W.-C. Chen, S.-W. Kuo and F.-C. Chang, *Polymer*, 2010, **51**, 4176–4184.
193 C. Tang, E. M. Lennon, G. H. Fredrickson, E. J. Kramer and C. J. Hawker, *Science*, 2008, **322**, 429–432.
194 Y. Zhuang, L. Wang and J. Lin, *J. Phys. Chem. B*, 2011, **115**, 7550–7560.
195 X. Zhang, J. Lin, L. Wang, L. Zhang, J. Lin and L. Gao, *Polymer*, 2015, **78**, 69–80.
196 C. Tang, S.-M. Hur, B. C. Stahl, K. Sivanandan, M. Dimitriou, E. Pressly, G. H. Fredrickson, E. J. Kramer and C. J. Hawker, *Macromolecules*, 2010, **43**, 2880–2889.
197 X. Zhang, L. Wang, T. Jiang and J. Lin, *J. Chem. Phys.*, 2013, **139**, 184901.
198 H.-S. Sun, C.-H. Lee, C.-S. Lai, H.-L. Chen, S.-H. Tung and W.-C. Chen, *Soft Matter*, 2011, **7**, 4198–4206.
199 N. Sary, F. Richard, C. Brochon, N. Leclerc, P. Lévêque, J. N. Audinot, S. Berson, T. Heiser, G. Hadziioannou and R. Mezzenga, *Adv. Mater.*, 2010, **22**, 763–768.
200 M. He, F. Qiu and Z. Lin, *J. Mater. Chem.*, 2011, **21**, 17039–17048.
201 L.-M. Chen, Z. Xu, Z. Hong and Y. Yang, *J. Mater. Chem.*, 2010, **20**, 2575–2598.
202 Y. Lee and E. D. Gomez, *Macromolecules*, 2015, **48**, 7385–7395.
203 H. Chen, Y.-C. Hsiao, B. Hu and M. Dadmun, *J. Mater. Chem. A*, 2014, **2**, 9883–9890.
204 C. Duan, R. E. Willems, J. J. van Franeker, B. J. Bruijnaers, M. M. Wienk and R. A. Janssen, *J. Mater. Chem. A*, 2016, **4**, 1855–1866.
205 G. A. Buxton and N. Clarke, *Modell. Simul. Mater. Sci. Eng.*, 2007, **15**, 13–26.
206 R. A. Marsh, C. Groves and N. C. Greenham, *J. Appl. Phys.*, 2007, **101**, 083509.
207 F. Yang and S. R. Forrest, *ACS Nano*, 2008, **2**, 1022–1032.
208 G. A. Buxton and N. Clarke, *Phys. Rev. B: Condens. Matter*, 2006, **74**, 085207.
209 M. Shah and V. Ganesan, *Macromolecules*, 2010, **43**, 543–552.
210 R. G. E. Kimber, A. B. Walker, G. E. Schröder-Turk and D. J. Cleaver, *Phys. Chem. Chem. Phys.*, 2010, **12**, 844–851.
211 S. Donets, A. Pershin, M. J. Christlmaier and S. A. Baeurle, *J. Chem. Phys.*, 2013, **138**, 094901.
212 Y. Tao, B. McCulloch, S. Kim and R. A. Segalman, *Soft Matter*, 2009, **5**, 4219–4230.
213 X. Cao, L. Zhang, J. Gu, L. Wang and J. Lin, *Polymer*, 2015, **72**, 10–20.
214 Y. Tao, H. Zohar, B. D. Olsen and R. A. Segalman, *Nano Lett.*, 2007, **7**, 2742–2746.
215 K. S. Yee, *IEEE Trans. Antennas Propag.*, 1966, **AP-14**, 302.
216 G. A. Buxton, J. Y. Lee and A. C. Balazs, *Macromolecules*, 2003, **36**, 9631–9637.
217 T. Sun, D. Zhu, Z. Yang, Z. Liu and Y. Liu, *Appl. Phys. B*, 2006, **82**, 89–92.
218 M. Stefik, S. Wang, R. Hovden, H. Sai, M. W. Tate, D. A. Muller, U. Steiner, S. M. Gruner and U. Wiesner, *J. Mater. Chem.*, 2012, **22**, 1078–1087.
219 J. A. Dolan, B. D. Wilts, S. Vignolini, J. J. Baumberg, U. Steiner and T. D. Wilkinson, *Adv. Opt. Mater.*, 2015, **3**, 12–32.
220 M. Stefik, S. Guldin, S. Vignolini, U. Wiesner and U. Steiner, *Chem. Soc. Rev.*, 2015, **44**, 5076–5091.

221 M. Maldovan, A. M. Urbas, N. Yufa, W. C. Carter and E. L. Thomas, *Phys. Rev. B: Condens. Matter*, 2002, **65**, 165123.
222 S. Vignolini, N. A. Yufa, P. S. Cunha, S. Guldin, I. Rushkin, M. Stefik, K. Hur, U. Wiesner, J. J. Baumberg and U. Steiner, *Adv. Mater.*, 2012, **24**, OP23–OP27.
223 S. S. Oh, A. Demetriadou, S. Wuestner and O. Hess, *Adv. Mater.*, 2013, **25**, 612–617.
224 S. Salvatore, A. Demetriadou, S. Vignolini, S. S. Oh, S. Wuestner, N. A. Yufa, M. Stefik, U. Wiesner, J. J. Baumberg, O. Hess and U. Steiner, *Adv. Mater.*, 2013, **25**, 2713–2716.
225 X. Zhu, L. Wang, J. Lin and L. Zhang, *ACS Nano*, 2010, **4**, 4979–4988.
226 C. Soto-Figueroa, M.-d.-R. Rodríguez-Hidalgo and J.-M. Martínez-Magadán, *Polymer*, 2005, **46**, 7485–7493.
227 J. T. Seitz, *J. Appl. Polym. Sci.*, 1993, **49**, 1331–1351.
228 S. Deng, Y. Huang, C. Lian, S. Xu, H. Liu and S. Lin, *Polymer*, 2014, **55**, 4776–4785.
229 A. J. Meuler, G. Fleury, M. A. Hillmyer and F. S. Bates, *Macromolecules*, 2008, **41**, 5809–5817.
230 G. Fleury and F. S. Bates, *Macromolecules*, 2009, **42**, 3598–3610.
231 G. Fleury and F. S. Bates, *Macromolecules*, 2009, **42**, 1691–1694.
232 X. Zhu, L. Wang and J. Lin, *Macromolecules*, 2011, **44**, 8314–8323.